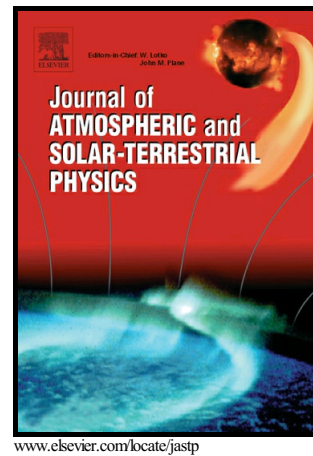


Author's Accepted Manuscript

Solar wind-atmospheric electricity-cloud
microphysics connections to weather and climate

Mai Mai Lam, Brian A. Tinsley



PII: S1364-6826(15)30081-X
DOI: <http://dx.doi.org/10.1016/j.jastp.2015.10.019>
Reference: ATP4306

To appear in: *Journal of Atmospheric and Solar-Terrestrial Physics*

Received date: 13 August 2015
Revised date: 16 October 2015
Accepted date: 23 October 2015

Cite this article as: Mai Mai Lam and Brian A. Tinsley, Solar wind-atmospheric electricity-cloud microphysics connections to weather and climate, *Journal of Atmospheric and Solar-Terrestrial Physics*, <http://dx.doi.org/10.1016/j.jastp.2015.10.019>

This is a PDF file of an unedited manuscript that has been accepted for publication. As a service to our customers we are providing this early version of the manuscript. The manuscript will undergo copyediting, typesetting, and review of the resulting galley proof before it is published in its final citable form. Please note that during the production process errors may be discovered which could affect the content, and all legal disclaimers that apply to the journal pertain

Solar wind-atmospheric electricity-cloud microphysics connections to weather and climate

Mai Mai Lam^{1*}, Brian A. Tinsley²

1. British Antarctic Survey, Cambridge, UK

2. University of Texas at Dallas, Richardson, TX, USA

ABSTRACT: We review recent research articles that present observations of the large-scale day-to-day dynamic tropospheric response to changes in the downward current density J_z of the global atmospheric electric circuit (GEC). The evidence for the global circuit downward current density, J_z , causing changes in atmospheric dynamics is now even stronger than as reviewed by Tinsley (Reports on Progress in Physics volume 71, 2008). We consider proposed mechanisms for these responses, and suggest future directions for research.

Keywords: solar wind; atmospheric electricity; cloud microphysics; weather and climate

1. INTRODUCTION

1.1 The global electric circuit (GEC) and the modulation of J_z and E_z

The world's thunderstorms and electrified clouds maintain a vertical electrical potential difference of about 250 kV between the ionosphere and the ground (e.g., Williams, 2005) as shown schematically in Fig. 1. The global electric circuit results from the upward current flow from these convective generators, spreading around the globe. The current returns to the surface as a downward current density J_z through the weakly ionized air and its embedded cloud and aerosol layers, where the associated vertical electric field is E_z . The ions are generated by the incoming galactic cosmic ray (GCR) flux, and their concentration decreases rapidly from the tropopause to the surface due to the attenuation of the GCR flux as it creates the ionization.

Our aim in this article is to provide a review of the observations of day-to-day meteorological effects correlating with J_z (typically a few pico-amperes per square metre), which shows variability with time and location over the globe. The action of the GEC on any timescale is of potential interest, and given present concerns about the effects of climate change on the planet, we are certainly interested in decadal scales and longer. However, the advantage of observing on daily timescales is that we can isolate the effects of the GEC on the atmosphere from the effects due to other mechanisms. There are a number of inputs to the atmosphere modulated by solar activity that all vary on the 11-year solar cycle, but on the day-to-day timescale their time variations are distinctly different. Also, in just a few years the day-to-day variations provide many events for evaluating the statistical significance of observed correlations. Furthermore, variability on the synoptic timescale of about 10 days may influence the development of longer term atmosphere-ocean variations such as the North Atlantic Oscillation (Hurrell et al., 2003, p. 16). Changes in the polar stratospheric vortex have been attributed to forcing by the upward propagation of planetary-scale Rossby waves originating in the troposphere (Andrews et al., 1987). In turn, downward dynamical propagation from the stratosphere on a timescale of months can affect longer term tropospheric dynamics and sea-surface temperature (Reichler et al., 2012). Thus there is a need to quantify short-term forcing and its long-term change in order to fully understand decadal and longer term climate changes.

*Corresponding author: Mai Mai Lam, Department of Meteorology, University of Reading, Earley Gate, PO Box 243, Reading, RG6 6BB, UK. maimailam7@gmail.com

The studies reviewed in this paper, therefore, are useful for probing the nature of the links between solar variability and the atmosphere, and we show that they provide strong evidence for the GEC being one such link. We also explore mechanisms for tropospheric responses, which are proposed to operate via the action of J_z producing space charge (non-zero net charge) in clouds and affecting cloud microphysics. Finally we consider possibilities for future research efforts in this area that could lead to further progress.

One longstanding obstacle for the plausibility of J_z (also of cosmic rays) as a driver for tropospheric dynamical responses has been the very large energy amplification needed (e.g., Willis, 1976; Lean and Rind, 1998). However, in cloud processes there is continual conversion from thermal energy to potential energy to latent heat release, with outcomes affecting either, or both of, the atmospheric dynamics and the atmospheric radiative balance. Very small energy inputs can divert the energy flow. Two such situations where energy flow can be modulated by cloud microphysical responses to J_z changes are as follows:

(1) The process of storm invigoration (e.g., Rosenfeld et al., 2008) occurs with changes in the concentration and size distribution of aerosol particles acting as cloud condensation nuclei (CCN), which results in changes in the droplet size distribution as updrafts create cooling and condensation. For increasing concentrations of smaller CCN compared to normal, the available water vapor is converted into increased concentrations of smaller droplets. The CCN act as a regulator of coagulation and precipitation processes; with smaller droplets, more liquid water is carried above the freezing level instead of precipitating, and the freezing releases more latent heat of freezing, which invigorates the updraft. Smaller numbers of large CCN are expected to have the same effect, because smaller numbers of larger droplets are formed, which also inhibits the coagulation and precipitation processes. In addition, increases in collision rates of ice forming nuclei (IFN) with liquid droplets above the freezing level can induce droplet freezing and also contribute to the release of latent heat of freezing and invigoration.

(2) Changes in cloud albedo, cloud cover, and infrared opacity affect regional radiative balance, indirectly affecting regional atmospheric dynamics (e.g., IPCC, 2013). This is applicable to layer clouds where the concentration and size distribution of droplets, responding to changes in cloud microphysics, act as a valve on the flow of radiation. The droplet size distribution affects albedo and infrared opacity directly and also indirectly affects cloud cover because of changes in drizzle production and cellular structure in broken clouds (e.g., Rosenfeld et al., 2006). Similarly in mixed phase (water plus ice) clouds, changes in the fraction of ice affect the infrared opacity (Prenni et al., 2007).

For both of the above situations, the CCN and IFN can be viewed as agents in the partitioning of the energy flows. We present evidence and qualitative theoretical analysis supporting the view that the electric charges produced by cosmic rays and moved by current flow in the GEC modulates the properties of the agents and their regulation of the energy flows.

2. REVIEW OF OBSERVATIONS

The large number of responses, on the day-to-day timescale, of the large-scale dynamics of the atmosphere that occur when regional changes occur in J_z , provide compelling evidence of a role for the GEC in weather and climate. The case for the action of J_z on atmospheric dynamics is now even stronger than when reviewed by Tinsley (2008), and consistent with the prescient remarks of Newell (1983). Fig. 2 presents a summary of such J_z -related meteorological effects and their proposed relationship to inputs to the GEC. Six independent forcing agents (A through F) are shown, all of which affect the ionosphere-earth current density J_z , along with proposed pathways to account for the meteorological responses that correlate independently with each of these inputs. The six forcing agents result in the following groups of responses: A - the Mansurov effect; B - the Burns effect; C and F - the Roberts, Pudovkin, and Egorova effects; D - the Wilcox, Kniveton, Roldugin, and Misumi effects; and E - the Schuurmans and Veretenenko effects. In the remainder of this section, we focus on (2.1) the Mansurov effect, (2.2) the Burns effect, (2.3) the Roberts effect, (2.4) the Wilcox effect, and (2.5) the Veretenenko effect. The Kniveton, Roldugin, Misumi, Schuurmans, Pudovkin and Egorova effects are described in Tinsley (2008). In this section, we give a review dealing mainly with new results, and new interpretations of old results, updating Tinsley (2008) and other reviews of this area (Rycroft et al., 2012; Gray et al. 2010).

2.1 The Mansurov effect

The Mansurov effect (Forcing Path A in Fig. 2) is a well-established correlation of polar surface pressure anomalies with solar-wind-driven changes in the polar cap ionospheric potential on the day-to-day timescale; specifically the potential variation maximizing at the magnetic poles driven by the north-south component (in geocentric solar magnetospheric or GSM co-ordinates) of the solar wind electric field $V_x B_y$. V_x is the solar wind radial velocity and B_y is the dawn-dusk component of the solar wind magnetic field (also known as the interplanetary magnetic field or IMF). Variations in $V_x B_y$ due to V_x are relatively small compared to those due to B_y because the latter reverses on timescales of 5 to 15 days as the solar wind sector structure, related to the location of coronal holes, passes over the Earth. The Mansurov effect has been demonstrated in data since the 1964 International Quiet Sun Year (IQSY) (Mansurov et al., 1974; Page, 1989; Tinsley and Heelis, 1993; Burns et al., 2007, 2008; Lam et al., 2013, 2014). This effect is the clearest and most direct example of a meteorological response to changes in J_z , with very high levels of statistical significance observed (e.g., Table 1 in Burns et al., 2008; Table 1 in Lam et al., 2013). These analyses have been made as a function of B_y alone, and even higher levels of statistical significance are to be expected for correlations made with the product $V_x B_y$. The Mansurov effect is illustrated in Fig. 3. Panel 3a shows the zonal mean anomaly in the surface pressure from National Centers for Environmental Prediction/National Center for Atmospheric Research (NCEP/NCAR) reanalysis data (Kalnay, 1996). This has been done for two distinctly different states of the IMF; when the daily average of IMF B_y is greater than, or equal to, 3 nT (red) and when it is less than, or equal to, -3 nT (blue). The difference between the red and the blue lines (Fig. 3b) highlights significant differences between the zonal mean surface pressure anomalies for the two IMF states in the polar regions. These are highly statistically-significant above about 60° latitude (at the 1% level), in both hemispheres (Fig. 3c).

No correlations of high latitude surface pressure with B_z have been found, and this can be understood in terms of the different dependency of the *daily average* polar cap ionospheric potential on IMF B_y , compared to its dependency on IMF B_z . The daily average contribution associated with the dawn-dusk component of the solar wind electric field, $V_x B_z$, is small at high geomagnetic latitudes because, although $V_x B_z$ has a strong influence on the electric potential drop, it is approximately equal and opposite on the dawn and dusk sides of the polar cap. Thus the B_z influence largely cancels out over the course of a day, with little day-to-day variability (Fig. 4b). In contrast, there is a significant spatial and IMF B_y -dependent *daily average* perturbation, of between -30 to +30 kV, to the vertical electrical potential drop of about 250 kV between the ground and the polar ionosphere (Fig. 3d-e, Fig. 5 and Fig. 4a), associated with the north-south (GSM) component of solar wind electric field. This B_y -related variation in the potential drop occurs at high geomagnetic latitudes ($> 74^\circ$ Corrected Geomagnetic Co-ordinates or CGM) and has a persistence time determined by the sector structure (5-15 days).

The recent work using reanalysis data, illustrated in Fig. 3, has confirmed and extended the spatial scope of the Mansurov effect previously shown in polar station data (Burns et al., 2007, 2008). A mid-latitude surface pressure influence of IMF B_y is also revealed. Specifically, the difference between the mean surface pressures during times of high positive and times of high negative IMF B_y possesses a statistically-significant mid-latitude wave structure similar to atmospheric quasi-stationary planetary-scale Rossby waves (Fig. 2 of Lam et al., 2013). The reason that this is of interest to the Sun-weather debate is that planetary waves have a key influence on weather. Quasi-stationary Rossby waves typically possess a zonal wavenumber of between about 3 and 7, and are therefore planetary in their spatial scale. These waves were first identified as ‘centers of action’ in the pressure systems found in weekly-mean sea level pressure charts (e.g. Rossby, 1940). At higher altitudes they no longer appear as closed isobaric systems, and appear as undulations in the jet stream (8 km altitude and above). Lam et al. (2013) propose that there will indeed be a solar-wind-driven modification to the Rossby wave field if one considers the generalization of the original theory of Rossby waves (Rossby et al., 1939) to the case of periodic variations in both longitude and latitude (Batchelor, 1967), for a fixed value of the longitudinal wavenumber. The direct effect on atmospheric pressure in the polar regions, along with the lack of effect on pressure at low latitudes, results in a change in the latitudinal sea-level pressure gradient in mid-latitude regions. In the generalized Rossby wave theory, a change in the mean zonal wind therefore results in a change in the meridional wavelength, which can account for the Rossby-wave-like form of the IMF-related pressure anomaly. The amplitude of the mid-latitude IMF B_y effect is

comparable to typical initial analysis uncertainties in ensemble numerical weather prediction (Buizza et al., 2010), which are known to be important to subsequent atmospheric evolution and forecasting (Isaksen et al., 2010). The Mansurov effect could therefore have an important effect, via the nonlinear evolution of atmospheric dynamics (Lorentz, 1963), on critical atmospheric processes. Indeed any mechanism that produces atmospheric responses to the solar wind in the polar regions could, in principle, modulate pre-existing weather patterns at mid-latitudes.

Another study using NCEP/NCAR reanalysis data (Lam et al., 2014) indicates that the atmospheric response of the Mansurov effect originates in the lower troposphere. Fig. 6 shows the altitude and time lag dependence of the correlation between IMF B_y and the geopotential height anomaly above Antarctica. The correlation is most statistically significant within the troposphere (Fig. 6b). The peak in the correlation occurs at greater time lags at the tropopause ($\sim 6-8$ days) and in the mid-troposphere (~ 4 days), than in the lower troposphere (~ 1 day) (Fig. 6c; Fig. 3 of Lam et al., 2014). This supports a mechanism involving the action of the global atmospheric electric circuit, modified by variations in the solar wind, on lower tropospheric clouds. The increase in time lag with increasing altitude is consistent with the upward propagation by conventional atmospheric processes of the solar-wind-induced variability in the lower troposphere. The relatively short timescale and the apparent upward propagation of this solar-wind-induced effect is in contrast to the downward propagation, on a timescale of months, of meteorological effects to the lower troposphere from the stratosphere due to other mechanisms associated with solar variability involving stratospheric ultraviolet (UV) radiation (e.g., Gray et al., 2010; Ineson et al., 2011; Ermolli et al., 2013) and precipitating energetic particles. Energetic particles, in the form of galactic cosmic rays, solar proton events (SPEs), and energetic electron precipitation from the aurora and the radiation belts associated with geomagnetic storms and substorms, are able to affect atmospheric chemical composition, dynamics, and climate (e.g., Rozanov et al., 2012; Seppälä et al., 2014; Mironova et al., 2015, and the paper by Georgieva et al. in this issue).

Both of the cloud processes (1) and (2) mentioned in the introduction could contribute to the Mansurov effect. The application of process (1), storm invigoration, would be in the upward branch of the Ferrell cell, in the vicinity of the ice-ocean interface. Modifications to the vertical current density of the GEC can also occur due to variations in the internal atmospheric thunderstorm generators. These generate day-to-day changes in J_z , to which there is an identical response of polar cap surface pressure (Forcing Path B), which provides strong corroboration for the solar wind influence via J_z (Burns et al., 2008). The Burns effect will be discussed in more detail in the next section (2.2).

2.2 The Burns Effect

The Burns effect (Forcing Path B in Fig. 2) is the observed correlation of the daily average of the surface atmospheric pressure with the daily average of the near-surface vertical electric potential gradient, PG (PG is an equivalent term for the downward electric field). Variability in these is proportional to changes in the overhead ionospheric potential, driven by variability in the sources, dominated by low-latitude thunderstorms and electrified showers. Burns et al. (2007, 2008) used PG values measured at Vostok station, high on the Antarctic plateau. This has proved to be a good location at which to measure PG, as it has stable, clean air with very few natural or anthropogenic aerosols, giving the PG a relatively high signal to noise ratio. Having corrected the PG by removing the small solar wind effect, the Burns effect was observed in 1998-2001 surface pressure data, with high statistical significance, at seven stations in the Arctic and eleven stations in the Antarctic. A persistence of 4-5 days and an amplitude of 3-5 hPa were observed. In contrast to the Mansurov effect where for a given IMF B_y change the ionospheric electric potential change, and therefore the pressure change, is opposite in the Arctic to that in the Antarctic, the Burns effect has the same sign of pressure change in both polar regions. The atmospheric sensitivity to IMF B_y (the Mansurov effect) was compared to its sensitivity to the internal thunderstorm-driven driver (Burns et al., 2008). Fig. 7 shows the similarity of the sensitivity of the two drivers in Antarctica for latitudes poleward of 83° magnetic latitude, and shows the larger range of the thunderstorm-driven response.

The meteorological generators of global ionospheric potential also have an effect away from the surface on the Vorticity Area Index (VAI). The VAI is an objective measure for the area of high cyclonic vorticity. A positive correlation exists at 500 hPa between small changes in high-latitude winter VAI ($60-80^\circ\text{N}$) and changes in current density J_z measured at the low-latitude Mauna Loa Observatory (Hebert et al., 2012).

Observations were not used when there were short-term decreases in the GCR flux, known as Forbush decreases, or for high stratospheric aerosol loading. Linear regressions of the lagged VAI anomalies with J_z values, for the winters of 1977-1982, have the largest values of R^2 , where R is the correlation coefficient, for a lag of +2 days. When 1960–1961 winters are examined, both the maximum slope and the maximum in the R^2 value occur at a lag of –3 days. However, the autocorrelation of VAI has a width of ~ 15 days, and the noise associated with the small number of data points in 1960–1961 will result in a displacement of the lag. The VAI responses were considered to be consistent with J_z as a driver, and thus with the high-latitude surface pressure response to variability of the daily-averaged J_z values (the Burns effect), and consistent with J_z being the driver for multiple effects: the Mansurov effect, the Roberts effect, the Wilcox effect and the Veretenenko effect.

Harrison and Ambaum (2013) have identified an effect of the diurnal variation in the global PG, known as the Carnegie curve, on the properties of layer clouds. Their study found a statistically-significant correlation between the ceilometer beam reflection height from the base of such clouds and the vertical ‘fair-weather’ electric field (Fig. 8), as specified by statistical empirical data (Torreson et al., 1946). This analysis was conducted during polar night to take advantage of the reduced variability due to solar radiation. The sensitivity of the ceilometer beam reflection height to the fair-weather electric field in the northern hemisphere is indistinguishable from that in the southern hemisphere, averaging at a (4.0 ± 0.5) m rise for a 1% change in the fair weather electric current density. This result suggests the variations in J_z , driven by variations in the global generator, can be linked to changes in layer cloud properties, by at least one pathway, on timescales of considerably less than a day.

2.3 The Roberts Effect

The Roberts effect (Forcing paths C and F in Fig. 2) was first observed as a correlation of surface pressure changes in winter storms with the occurrence of geomagnetic storms (Duell and Duell, 1948; Macdonald and Roberts, 1960). The effect is evaluated more objectively from gridded meteorological data sets in terms of computed changes in the areas of high tropospheric vorticity in winter at mid-high latitudes (Roberts and Olsen, 1973; Padgoanker and Arora, 1981). The vorticity reductions during magnetic storms are also associated with Forbush decreases, which are caused by coronal mass ejections (CMEs) reaching the Earth, and which also cause most large geomagnetic storms. Initially the underlying cause of the Roberts effect was proposed to be changes in atmospheric ionization due to the reduction of the GCR flux, (Tinsley et al., 1989; Tinsley and Deen, 1991), but consideration of the Mansurov effect by Tinsley and Heelis (1993), in which there is a change in J_z but no change in atmospheric ionization, prompted a reinterpretation of the Roberts effect as also driven by changes in J_z . There are strong theoretical expectations of high-latitude J_z reductions with Forbush decreases of GCR (Tzur et al., 1983; Roble and Tzur, 1986), but in practice there are limited direct measurements of J_z during these events. In addition, difficulties arise in selecting events for analysis because the CMEs that produce Forbush decreases are sometimes accompanied by solar energetic particles (SEPs), by changes in the high latitude ionospheric potential, and by changes in relativistic electron precipitation. Another way in which J_z reductions can arise during magnetic storms is through changes in ionospheric potential at sub-auroral latitudes. The negative potential changes occur with sub-auroral polarization streams (Foster and Vo, 2012) and sub-auroral ion drifts (Anderson et al., 2001).

The response in the geopotential height to Forbush decreases of GCR flux (Forcing path F) was investigated by Artamonova and Veretenenko (2014). In this study, a superposed epoch analysis was conducted in both hemispheres, using NCEP/NCAR reanalysis data from 1980-2006 at 1000 hPa for October-March. Although this is a warm period for the southern hemisphere, the authors note that significant horizontal temperature contrasts at polar fronts still exist over the South Atlantic and the Indian Ocean, and that these contribute to cyclonic activity. An increase in pressure following Forbush decreases was observed at mid-latitudes ($40\text{--}70^\circ$) in both hemispheres, which was accompanied by a decrease in pressure at high latitudes. In the northern hemisphere, a growth in the pressure, that peaked on days 3-4 of the superposed epoch analysis, occurred over Northern Europe and European Russia, as first seen in Artamonova and Veretenenko (2011). In the southern hemisphere, two regions of pronounced pressure growth were found which peaked on days 4–5. The first region was located over the eastern part of the South Atlantic and the second one was over the D’Urville Sea in the Southern Ocean. The most pronounced pressure deviations were associated with climatic Arctic/Antarctic and polar fronts (Fig. 9), which are regions of intensive cyclonic

activity. According to a weather chart analysis, the detected pressure increases are due to the weakening of cyclones and intensification of anticyclones at extratropical latitudes in both hemispheres. Since changes in sub-auroral ionospheric potentials generally accompany those Forbush decreases which are associated with magnetic storms, the relative importance of these two forcing agents (C and F in Fig. 2) for the responses observed by Artamonova and Veretenenko (2011, 2014), and responses to magnetic storms generally, has not been determined.

2.4 The Wilcox Effect

The Wilcox effect was first observed as a reduction in the areas of high vorticity in winter storms at times of solar wind heliospheric current sheet (HCS) crossings (Wilcox et al., 1973; Hines and Halevy, 1977; Larsen and Kelly, 1977). These were later shown to be more directly correlated with reductions in the quasi-trapped relativistic electron flux (REF) (Forcing path D in Fig.2) precipitating from the radiation belts at sub-auroral latitudes. It was shown that the strength of the effect depends on the amount of sulfuric acid aerosol in the middle atmosphere, which is estimated to decrease middle atmosphere conductivity, and therefore J_z , for a few years after volcanic injection of sulfur (Tinsley et al., 1994; Kirkland et al., 1996; Tinsley and Zhou, 2006), provided there is not a countering increase in ionization due to relativistic electron precipitation. This scenario is supported by some historic J_z observations which included periods with large volcanic eruptions (Reiter, 1977; Fischer and Mühleisen, 1980). Decreases in the REF, which produce decreases in middle atmosphere ionization and therefore decreases in J_z , can be considered responsible for the decreases in vorticity observed in the Wilcox effect. J_z modulation by the REF requires that R_M is not negligible with respect to R_T (Fig. 1). J_z modulation, and a response in the area of high vorticity, appear when the stratospheric aerosol content is very high, or when the REF reductions are very deep and, very approximately, when the product of the stratospheric aerosol content and the reciprocal of the REF exceeds a threshold value dependent on R_T . As with the Mansurov effect, there are no correlated changes in tropospheric ionization at HCS crossings, leaving J_z changes as the only candidate for a driver.

Recent work has confirmed these relationships. The Vorticity Area Index (VAI) has generally been used, and in recent studies, it was derived from ERA-40 and ERA-Interim reanalyses of global meteorological data. During winters for the period 1957-2011, the vorticity changes were greater for winters with higher levels of stratospheric volcanic aerosols; in addition, when days of minima in the REF are used instead of HCS crossings as key days in the superposed epoch analyses, the ability to detect vorticity changes is improved (Tinsley et al. 2012; Mironova et al., 2012b). Zhou et al. (2014) showed the effect of minima in solar wind speed and the geo-effective interplanetary electric field which modulate the REF (e.g. Gao et al., 2015) on day-to-day changes in the North Atlantic Oscillation (NAO) Index and the Arctic Oscillation (AO) Index.

2.5 The Veretenenko Effect

The Veretenenko effect is the observed increase in tropospheric vorticity that accompanies solar energetic particle (SEP) events (also known as solar proton events, SPEs). This effect is associated with an increase in J_z which we propose modifies the atmosphere via the processes associated with Forcing path E (Fig. 2). Increases in areas of high vorticity in winter storms, at times and locations of SEP events, were observed near Greenland by Veretenenko and Thejll (2004, 2005). The responses were seen during stronger events, such as Ground Level Events (GLEs), which produce increases in ionization into the troposphere. Models show that reduced column resistance and increased J_z occur for such events (Roble and Tzur, 1986).

Recently, empirical evidence has been produced for a possible effect of the ionization associated with an extreme SEP event on stratospheric aerosols (Mironova et al., 2012a). Significant simultaneous changes in aerosol properties were found in the polar stratosphere (11-25 km) of both hemispheres. Polar aerosol data were used, from the Stratospheric Aerosol and Gas Experiment (SAGE) III and from the Optical Spectrograph and Infrared Imaging System (OSIRIS), collected during the extreme SEP event which occurred on 20 January 2005. The change in aerosol properties, though only marginally detectable for this severe SEP event, is statistically robust. The authors speculate that the abnormally high ionization of the lower stratosphere in the polar regions during this SEP event may have led to the formation of new ultrafine aerosol particles (by ion-mediated nucleation (Dickinson, 1975; Kirkby et al., 2011) and/or to the growth of pre-existing ultrafine particles.

Having found an intensification of cyclone regeneration in the North Atlantic associated with SEPs, using both NCEP/NCAR reanalysis data and weather charts (Veretenenko and Thejll, 2004; 2005), Veretenenko and Thejll (2013) studied variations in cyclonic activity at middle latitudes associated with SEP events where particle energies exceeded 90 MeV, using the reanalysis data from both hemispheres. A superposed epoch analysis of such events showed noticeable intensification of cyclonic activity, mainly over the oceans during the colder half of the year. In the northern hemisphere, this intensification was observed for October-March, while in the southern hemisphere, the intensification was most pronounced for April-September. For each hemisphere, the largest intensification in winter cyclones takes place in regions characterized by large meridional temperature contrasts (generating baroclinic instabilities) and low values in the geomagnetic cut-off rigidity. The cut-off rigidity is a measure of the shielding provided by the Earth's magnetic field from energetic charged particles passing through the magnetosphere towards the ground. A weaker horizontal component of the geomagnetic field allows greater fluxes of SEPs to penetrate and to ionize the atmosphere. The short-term response to increases in SEP flux has been directly compared with that due to decreases in GCR flux by Artamonova and Veretenenko (2013). They found contrasting changes in the zonal and meridional circulation patterns, classified by type in a catalogue of macroscopic processes which is available from 1964 onwards (Vangengeim, 1964).

Our review of observations leads us to regard the evidence for tropospheric responses to J_z changes as compelling. Firstly, this is because the correlations are on the day-to-day time-scale so that, although the amplitude of the responses is small, the availability of tens to hundreds of events ensure that very high statistical significance has been demonstrated. Secondly, we have reviewed in this section six different types of inputs to the global circuit that cause day-to-day variability of J_z , and the responses agree in onset time, duration, amplitude, location and sign of response with each of these variations (although there is an ambiguity for the Roberts effect). The inputs are (2.1) the solar wind speed and interplanetary magnetic field components affecting polar cap ionospheric potentials, (2.2) the current output of the thunderstorm and electrified cloud generators, (2.3) coronal mass ejections affecting sub-auroral ionospheric potentials and galactic cosmic rays, (2.4) relativistic electrons from the radiation belts, and (2.5) solar energetic particles (SEPs).

3. PROPOSED MECHANISMS FOR TROPOSPHERIC RESPONSES

While ion-mediated nucleation of condensation nuclei on cosmic-ray produced ions (Dickinson, 1975; Carslaw et al., 2002; Kirkby et al., 2011) has been postulated as a source for CCN and cloud microphysical changes related to Forbush decreases and 11-year cycles of GCRs, it cannot account for the Mansurov, Burns, Veretenenko or Wilcox effects. For these, there is no correlated change in cosmic ray flux and ion production in the lower troposphere, where the responses of cloud cover and vorticity are seen (there can be changes in ionization in the middle atmosphere that modulate J_z).

As noted in the introduction, in cloud processes there is continual conversion of energy between thermal energy, latent heat, gravitational potential energy and dynamical energy, and the partitioning can be affected by very small energy inputs. A sequence of two processes has been proposed.

The first is the accumulation of charge on droplets and aerosol particles - most importantly, cloud condensation nuclei (CCN) and ice forming nuclei (IFN) - due to the ionization by cosmic rays and the flow of current density (J_z) through clouds and aerosol layers (Fig. 10). There have been many measurements of droplet charges in clouds (e.g., Pruppacher and Klett, 1997, section 18.4). For clouds and aerosol layers without deep convection, net average positive charges are found on droplets at upper boundaries and net negative charges at lower boundaries. This is consistent with space charge accumulation required by Poisson's equation, as J_z flows through conductivity gradients (e.g., at boundaries of cloud or aerosol layers) and creates electric field gradients.

Models of the charging of layer clouds have been made by Zhou and Tinsley (2007, 2012). There is a need to extend these to three dimensions for application to convection in the cellular structure of marine stratocumuli. For convective clouds, charged aerosols from near the surface, with charge originating with J_z , are carried by the updrafts into the body of the cloud. Observations provide a starting point for models, and experiments and outlines of the processes can provide some guidance (Vonnegut et al., 1962; Tinsley,

2012).

The second in the sequence of processes involves changes in scavenging rates by cloud droplets of aerosol particles – most importantly CCN and IFN – due to the electric charge on the particles and/or droplets. A discussion of models of such scavenging is given in the next section. Scavenging is due to collisions between the nuclei and droplets, entailing size-dependent collection of nuclei and changes in their size distribution and overall concentration. It affects a number of microphysical processes which cause changes in macroscopic cloud properties and partitioning of energy flow in the system. As noted in the introduction, two such situations where energy flow can be modulated by cloud microphysical responses to J_z changes are amplification by storm invigoration and by changes in cloud albedo, cloud cover, and infrared opacity.

3.1 Simulations of electro-scavenging and electro-anti-scavenging processes

Models of electrical effects on droplet-aerosol scavenging processes have been made, building on the work of Pruppacher and his students in the 1970s (Pruppacher and Klett, 1997). Scavenging is the removal of aerosol particles from the air inside or below a cloud, as collisions with droplets incorporate them into the droplets. This is important for changing concentrations and size distributions of CCN, and for production of ice. In the latter case, collisions of IFN with droplets below freezing temperatures result in contact ice nucleation, and collisions with warmer droplets provide immersion ice nuclei for freezing when droplets cool to below freezing temperatures. Trajectory simulations to determine scavenging rates (applicable to both in-cloud and below-cloud scavenging) have been made, without considering diffusion, by Tinsley et al. (2000, 2001), Tripathi and Harrison (2002), Tinsley et al. (2006), Tripathi et al. (2006), and Zhou et al. (2009). Trajectory simulations incorporating Brownian diffusion of the aerosol particles in the vicinity of the droplet, which dominates collisions for smaller particles interacting with droplets, have been made by Tinsley (2010). Below-cloud scavenging has been reviewed by Chate et al. (2011).

For use in cloud models, it is necessary to parameterize the results of simulations, since the computer time to make simulations during model runs would be impossibly long. The parameterizations of Tripathi et al. (2006) were for droplet sizes which were considerably larger than those typical for in-cloud scavenging, and did not include particle diffusion. The first parameterizations of simulations with diffusion are due to Tinsley and Leddon (2013), and now more accurate and user-friendly parameterizations are available (Tinsley and Zhou, 2015). Together with realistic models of cloud charging, these parameterizations provide the inputs for use as model scavenging rates in realistic models of cloud formation and development.

Fig. 11 shows results of simulations by Tinsley and Zhou (2015) for the variation of scavenging rate in terms of a function $F = \log(R_{Q,q}/R_{0,0})$, for droplets of radius $6\ \mu\text{m}$ and for three aerosol particle radii, $0.01\ \mu\text{m}$, $0.04\ \mu\text{m}$, and $1.5\ \mu\text{m}$. $R_{Q,q}$ is the rate coefficient for droplet charge Q and aerosol particle charge q , and $R_{0,0}$ is the rate coefficient for zero droplet and particle charges. The abscissa in each plot is Q , from $-100e$ to $+100e$, and the ordinates are q , from $1e$ to $50e$, where e is the elementary charge ($1.6 \times 10^{-19}\ \text{C}$). For small particles, as in Fig. 11 for $a = 0.01\ \mu\text{m}$, with Q and q having opposite sign, there can be strong increases in the scavenging rate coefficient (electro-scavenging) relative to uncharged droplets or particles, and for Q and q of the same sign, there can be strong decreases in scavenging rates (electro-anti-scavenging). This is due to the long-range Coulomb force, proportional to Qq , being repulsive or attractive depending on the signs of Q and q . For the larger particles, the short-range image charge attraction generated by q dominates, and this can be seen in the small tilt of the contours in Fig. 11. For zero Q (the central vertical lines) there is always an increase in the rate. Also, there is an effect of the short-range attraction due to the dipole induced by Q on the particle. For $a = 1.5\ \mu\text{m}$ in Fig. 11, this can be seen as the light blue area of positive F near the lower right hand corner, standing in contrast to the negative F (darker blue) of the moderate Coulomb repulsion with small values of q .

Thus for CCN, electric charge can increase or decrease the scavenging rates, depending on CCN size and charge, and change the concentrations and size distributions of the CCN, leading to size dependent changes in droplet concentration important in later episodes of condensation. For the larger CCN, electro-scavenging proceeds even in regions with no net space charge, i.e., with equal number of positive and negative charges, since the image charge attraction is independent of whether Q and q have the same sign

(seen along the central vertical axes in Fig. 11). Thus, electro-scavenging of large CCN always reduces their concentration. This could lead to a response of clouds to changes in ion production by GCR flux changes, as in the Roberts effect, even if J_z remained constant. However, J_z generally changes when GCR flux changes, so there are no observational data to test this.

For IFN the most effective nuclei are relatively large, and again, only increases in scavenging rates occur. In clouds above the freezing level, scavenging by supercooled droplets results in contact ice nucleation, i.e., freezing of the droplet which can then grow rapidly by the Wegener-Bergeron-Findeisen process (Fleagle and Businger, 1980) taking up water vapor. This lowers the vapor pressure and causes nearby droplets to evaporate ('glaciating' the cloud).

As noted above in the Introduction under points (1) and (2), such processes can affect the macroscopic properties of storm clouds by latent heat release and the storm invigoration process, and affect layer clouds by changes in droplet size distribution leading to changes in cloud albedo, infrared opacity, and cloud cover. It remains for modelling of the magnitude of such effects to test whether these can account for the observed responses to J_z changes.

For IFN the most effective nuclei are relatively large, and again, only increases in scavenging rates occur. In clouds above the freezing level, scavenging by supercooled droplets results in contact ice nucleation, i.e., freezing of the droplet, which can then grow rapidly by the Wegener-Bergeron-Findeisen process, taking up water vapor which lowers the vapor pressure and causing nearby droplets to evaporate, ('glaciating' the cloud).

3.2 Time scales for charging and scavenging

The ionization produced in the global atmosphere by the cosmic ray flux moves to form the downward current density J_z in the global electric circuit, with the positive and negative air ions flowing downward and upward respectively in the downward electric field (Fig. 1). The cosmic ray flux is strongly attenuated coming into the lower atmosphere, giving strongly decreasing conductivity with decreasing altitude. As J_z flows through conductivity gradients, it produces gradients in electric field and space charge in accordance with Ohm's Law and Gauss's Law. The conductivity gradients are greatest at the lowest altitudes, and half of the potential drop from the surface to the ionosphere in clear air is in the lowest 5 km (Roble and Tzur, 1986), so that most of the space charge accumulates in the lower troposphere. Layers of space charge occur at the tops and bottoms of layer clouds, owing to the low conductivity due to ion attachment to droplets in clouds, and in haze layers (Fig 10) as noted above. In addition, there is always a layer of space charge near the surface, whether it is land, ocean or ice. This is termed the 'electrode' effect, because the ion production of cosmic rays (and radon for the lowest one or two km over land) supplies downward moving positive ions above the surface, but not upward moving negative ions from below the surface, and to maintain downward current continuity, the concentration of positive ions must roughly double, and that of negative ions become relatively small, producing a layer of space charge (Hoppel et al., 1986; Gringel et al., 1986). The drift speed of air ions in the typical 100 V/m electric field near the surface is about 3 cm/sec, which is about the speed at which snowflakes fall. This determines the time scale for attaining equilibrium in space charge (the relaxation time), which is about ten minutes (Roble and Tzur, 1986). This is why convection and turbulence moving the space charge around near the surface is a source of noise for vertical electric field (E_z) measurements, except when the air with its stratified space charge is exceptionally stable. In general, the space charge inhomogeneities affect E_z at distances of tens to hundreds of metres, with greater distances for the larger sources such as large-scale convection, and stronger sources such as thunderstorms. J_z measurements have the advantage over E_z measurements for monitoring global circuit variations in that the equilibrium downward current density is due to the product of $V_1 R$, where R is the total column resistance to the ionosphere, which is less variable than the near-surface resistivity and space charge. However J_z is measured as a local collection of ions by an electrode, and in non-equilibrium conditions is more subject to the smallest scale inhomogeneities than E_z . The very long (600 metre) wire collector at a height of 10 metres used at the Borok Geophysical observatory (Anisimov et al., 2014) is one approach to this problem, which works well when the air is stable in winter.

The transfer of charge from the ions initially produced by cosmic rays (mainly N_2^+ and electrons) to

aerosol particles takes only microseconds for the electrons to attach to O_2 molecules, and milliseconds for these ions to attract polar molecules to become light cluster ions, or ‘air ions’ (Hoppel et al., 1986; Gringel et al., 1986). The time scales for the response of the charges on droplets and particles to a change in air ion concentration was found to range from about a minute to an hour, being smaller at higher altitudes than at low altitudes, and larger for larger aerosol concentrations (Zhou and Tinsley, 2012). At equilibrium, and in the absence of space charge, typical values for the ratio of concentrations of positively charged aerosol particles to neutral particles of the same size are about one to three, and the negative/neutral particle ratio is about one to two (Zhou and Tinsley, 2007). In the presence of space charge, the ratio of concentrations of particles in the positive, negative, and neutral states shifts toward an equilibrium dependent on the magnitude and sign of the space charge (Tripathi and Harrison, 2002).

The time scale for the response of aerosol concentrations to changes in aerosol scavenging caused by the electric charges on particles and droplets was found to be a few hours (Tinsley, 2010), for particle and droplet charges similar to those in Fig. 11. The time scale is particularly short for highly charged residues of evaporated droplets during the ten minutes or so that the high charge remains on them, and Beard (1992) noted that this would make them effective as contact nuclei in initiating ice production. Thus, evaporation of charged droplets in downdrafts and in air entrained by turbulence near cloud boundaries results in highly charged evaporation nuclei, as the charges and material absorbed by the droplet during its lifetime stay with it as it shrinks by evaporation. This material can activate the surface of the former CCN for ice nucleation (Rosinski and Morgan, 1991).

3.3 Pathways from microphysical to cloud-scale change.

Building on the outline given in the Introduction, we describe a number of ways in which the electric charges on aerosol particles and droplets (gained by attachment of the air ions produced by cosmic rays) can affect the microphysics and subsequent development of clouds. Water vapor condenses on CCN to form cloud droplets, and subsequently the droplets freeze, if the temperature is below freezing and there are available IFN that can encounter the droplet (these are needed unless the temperature is below about -30°C). There are two major categories of clouds to consider, and in both it is variations in the rate of conversion of liquid droplets to ice crystals where electrical charges on the CCN and IFN have a key role to play. The first category is clouds with vertical development due to updrafts, such as in cyclones and summer convective clouds. The second category is layer clouds, such as mixed phase (water and ice) at high latitudes and/or high altitudes (cirrus).

Responses to inferred J_z changes of high altitude clouds are found all year: with Forbush decreases by Todd and Kniveton (2001); and with relativistic electrons by Kniveton and Tinsley (2004) and by Roldugin and Tinsley (2004). However effects on cyclones in the northern hemisphere are confined to winter (sections 2.3, 2.4, and 2.5). Thus the effects on high altitude clouds cannot be a consequence of changes in storm dynamics. For cyclonic-type responses in the southern hemisphere, as found by Artamonova and Veretenenko (2013) and illustrated in Fig. 9, the effects occur in the southern summer. There, the stable anticyclone over the Antarctic continent is perturbed by katabatic outflows from the ice plateau, generating clouds with vertical development, susceptible to electrical effects on the cloud microphysics and storm system development.

The following pathways may apply to both layer clouds and to clouds with vertical development. The question of which pathways are most important for a given type of cloud could be resolved by a combination of modelling and in-situ measurements.

Pathway 1 is for charge effects on CCN concentrations and size distributions. Increases in scavenging rate - ‘electro-scavenging’ - for CCN larger than about $0.3 \mu\text{m}$ radius decreases their concentration independent of the sign of Q/q . With space charge present, decreases in scavenging rate - ‘electro-anti-scavenging’ - for smaller CCN result in concentrations remaining higher than without space charge. The lifetime of CCN in an air mass is one to ten days. In later cycles of evaporation/condensation, the CCN changes produce decreases of the concentration of large droplets and increase in those of small droplets. These reduce the rate of coagulation and initial precipitation, and updrafts carry more droplets above the freezing level. This produces more ice and the latent heat release increases the vigor (e.g., Rosenfeld et al.,

2008) and therefore the vorticity of baroclinic storms. It may also increase the amount of water released into the upper troposphere and change cloud cover and increase lightning. Also, as noted above, evaporation and production of highly charged residues occurs during entrainment, and in turbulent regions at cloud tops, and in below-cloud scavenging as small charged drizzle droplets evaporate while larger droplets are falling past them. The high charge on these residues changes their rate of being scavenged and thus the CCN size distribution.

Pathway 2 is for charged IFN in contact ice nucleation. IFN are generally larger than $0.5 \mu\text{m}$ radius: electro-scavenging increases the collision rate independent of the sign of Q/q . As droplets cool in updrafts, contact ice nucleation occurs at around -5°C in advance of other droplet freezing processes at around -15°C . With greater initial ice production, and increased latent heat of freezing, increased updraft speed (storm invigoration) occurs. For layer clouds there may be cloud cover changes.

Pathway 3 is for charged evaporation residues acting as IFN. As noted above, evaporation residues have relatively large charges on them for ten minutes or so, and some evaporation residues retain coatings which sensitize them as IFN. Thus, in clouds above the freezing level, highly charged evaporation nuclei can act as IFN in contact ice nucleation, promoting freezing.

Pathway 4 is for charge effects on in-cloud scavenging of IFN that later act as immersion nuclei. The particles that act as IFN but not as CCN are left as interstitial particles when cloud droplets are condensing on CCN. The interstitial IFN are electro-scavenged into droplets below the freezing level, and act as immersion IFN when the cloudy air rises above the -15°C level.

More speculative pathways involve ion-mediated nucleation of ultrafine particles (Dickinson, 1975; Kirkby et al., 2011) at altitudes and latitudes where CCN concentrations are low. In the presence of space charge at cloud boundaries, the ultrafine particles can grow with volatiles released from evaporating droplets at these boundaries. Electro-anti-scavenging may protect the ultrafine nuclei from coagulation as they grow by vapor deposition, until they are large enough to become CCN.

4. RECOMMENDATIONS FOR FUTURE WORK

4.1 *Observations needed*

A major problem for testing the mechanism for global electrical effects on clouds and atmospheric dynamics has been the difficulty of measuring large-scale temporal and spatial variations in E_z and J_z . The multitude of land surface measurements that have been made detect variations mainly due to local meteorology (convection, turbulence, variable aerosol and cloud perturbations, and thunderstorms). Balloon, aircraft and unmanned aerial vehicle (UAV) measurements get above near-surface disturbances, but are intermittent and expensive for long-term studies. However, it is now recognized that particular surface sites at high altitudes have exceptionally stable and clean air, and have much less local meteorological interference in the detection of the large-scale atmospheric electricity variations. Two such sites are Vostok, and Concordia, at about 3 km altitude on the Antarctic ice plateau. These are sites with exceptionally stable air, as they are in the downward branch of the Ferrell Cell of atmospheric circulation, and so washed by clean, dry stratospheric air. This also applies to South Pole, with the difference that that site is under the auroral oval, and therefore the large ionospheric potential changes due to B_z would have to be removed using, for instance, the method of removal of smaller solar wind-induced potential changes performed by Burns et al. (2007, 2008). On the other hand, the ionospheric potential changes are absolutely calibrated by radar and satellite measurements, and could be used (on a statistical basis) to absolutely calibrate E_z measurements. This would give absolute ionospheric potentials due to the internal atmospheric generators, independent of E_z variations due to seasonally changing near-surface conductivity. We recommend a continuing program of measurements at two or more of these sites.

We recommend the establishment of low-latitude stations at optimal sites. We suggest Atacama in the Chilean Altiplano. Like the Antarctic stations, it is at high altitude, and washed by descending stratospheric air, in this case the downward branch of the Hadley cell. It has excellent infrastructure due to the astronomical observatories, and exceptionally stable high-altitude atmospheric conditions at night. A flat expanse at high altitudes in descending air is optimal. The higher ion mobility at higher altitudes dissipates space charge inhomogeneities faster, and there are usually low water vapor and anthropogenic aerosol

concentrations. Shield volcanos such as Mauna Loa are also good sites, and areas close to the summit would avoid the effect of rising afternoon clouds and the turbulence due to katabatic winds moving over irregular surfaces on the slopes. There may be good sites in northern Tibet as well. Oceans and lakes have more stable air in daytime than land, and this suggests floating lake observatories, e.g., on Lake Titicaca in the Andes. There is a need to maintain observations at several such optimum sites at low latitudes, spaced in longitude for continuous overlapping observations with redundancy for poor atmospheric stability conditions, as well as one or two sub-auroral and polar stations, perhaps using UAVs. The longitudinal spacing would provide optimum data for day-to-day variations in the output of the internal generators, and the latitudinal spacing would allow separation of effects of solar modulated sources from those of the internal atmospheric meteorological generators. An international coordinated effort is required, and optimally the observational data could be incorporated, in real time, into an assimilative model of the global circuit, incorporating global meteorological data.

4.2 Modelling needed

Fig. 12 sets out the needs for quantitative modelling to test which of the pathways identified above in section 3.3 are most effective, and to test them quantitatively against observations. Separate modelling efforts will be needed for layer clouds compared to clouds with significant vertical development. If agreement with observations is found, the processes could be incorporated in global circulation models for forecasting the contributions of atmospheric electricity to weather and climate changes.

5. SUMMARY AND IMPLICATIONS

There is strong evidence for atmospheric dynamical responses to current density (J_z) changes in the global electric circuit. These are consistent with a mechanism, which we have outlined, involving electrical charging of aerosol particles (including CCN and IFN) and droplets in clouds, which modulates the rates of scavenging and the concentrations and size distributions of these nuclei. The changes in the nuclei in turn modulate the resulting droplet concentrations and size distributions, and affect ice production and the partitioning of atmospheric energy conversions between latent heat and kinetic energy and, with cloud cover changes, the partitioning of the short-wave and long-wave radiative transfer.

There is a need for quantitative modeling of these processes, to determine which of a number of microphysical pathways are most effective, and to provide quantitative results to compare with observations.

The day-to-day variability in J_z due to the thunderstorm generators is several times greater than that of the solar wind source, and is present at all latitudes, and so it is to be expected that it would contribute by the same physical processes described above as for the solar input, but with larger amplitude. The atmospheric responses (discussed in sections 2.1 to 2.5) to changes of only tens of percent in J_z are small, but imply that the overall level of J_z continually affects basic aerosol-cloud physics, because it is five or more times larger than the variable component. At this stage of our understanding we see no reason why such short-term responses should not be present on longer time scales, such as the 11-year and longer solar cycles in the solar wind and cosmic rays. With increases in J_z expected as the cosmic ray flux increases in another Maunder Minimum, effects on clouds and climate could be even greater in the future.

ACKNOWLEDGMENTS

BAT was supported by NSF grant AGS 0836171 and by NSFC grant 41271054. MML was supported by NERC grant NE/I024852/1 and by funds from a Philip Leverhulme Prize from the Leverhulme Trust. We gratefully acknowledge the support of the International Space Science Institute (ISSI), and of the EU COST action TOSCA which funded our attendance at meetings which contributed to useful discussions of this work. We thank two reviewers for constructive comments.

APPENDIX: ACRONYMS

AO: Arctic Oscillation
 CCN: cloud condensation nuclei
 CME: coronal mass ejections
 GCR: galactic cosmic ray
 GEC: global atmospheric electric circuit
 HCS: heliospheric current sheet
 IFN: ice-forming nuclei
 IMF: interplanetary magnetic field
 NAO: North Atlantic Oscillation
 NCAR: National Center for Atmospheric Research
 NCEP: National Centers for Environmental Prediction
 PG: potential gradient
 REF: relativistic electron flux
 SEP: solar energetic particles
 SPE: solar proton event
 UAV: unmanned aerial vehicle
 UV: ultraviolet
 VAI: Vorticity Area Index
 WRS: Wilcoxon Rank Sum

REFERENCES

- Anderson, P.C., Carpenter, D.L., Tsuruda, K., Mukai, T., Rich, F.J., 2001. Multisatellite observations of rapid subauroral ion drifts (SAID). *J. Geophys. Res.* 106(A12), 29585-29599, doi:10.1029/2001JA000128.
- Andrews, D.G., Holton, J.R., Leovy, C.B., 1987. *Middle Atmosphere Dynamics*, Academic Press, San Diego, USA, pp. 489.
- Anisimov, S.V., Galichenko, S.V., Shikhova, N.M., 2014. Space charge and electrostatic flows in the exchange layer: An experimental and numerical study. *Atmos. Res.* 135-136, 244-254, doi:10.1016/j.atmosres.2013.01.012.
- Artamonova, I., Veretenenko, S., 2011. Galactic cosmic ray variation influence on baric system dynamics at middle latitudes. *J. Atmos. Sol.-Terr. Phys.* 73(2-3), 366-370, doi:10.1016/j.jastp.2010.05.004.
- Artamonova, I.V., Veretenenko, S.V., 2013. Effect of solar and galactic cosmic rays on the duration of macrosynoptic processes. *Geomag. Aeron* 53(1), 5-9. doi: 10.1134/S0016793213010039.
- Artamonova, I., Veretenenko, S., 2014. Atmospheric pressure variations at extratropical latitudes associated with Forbush decreases of galactic cosmic rays. *J. Adv. Space Res.* 54(12), 2491-2498, doi:10.1016/j.asr.2013.11.057.
- Batchelor, G.K., 1967. *An Introduction to Fluid Dynamics*, Cambridge University Press, London, pp. 577-80.
- Beard, K.V., 1992. Ice initiation in warm-base convective clouds: an assessment of microphysical mechanisms. *Atmos. Res.* 28, 125-152.
- Buizza, R., Leutbecher, M., Isaksen, I., Haseler, J., 2010. Combined use of EDA- and SV-based perturbations in the EPS. *ECMWF Newsl.* 123, 22-8.
- Burns, G.B., Tinsley, B.A., Frank-Kamenetsky, A.V., Bering, E.A., 2007. Interplanetary magnetic field and atmospheric electric circuit influences on ground-level pressure at Vostok. *J. Geophys. Res.* 112, D04103, doi:10.1029/2006JD007246.
- Burns, G.B., Tinsley, B.A., French, W.J.R., Troshichev, O.A., Frank-Kamenetsky, A.V., 2008. Atmospheric circuit influences on ground-level pressure in the Antarctic and Arctic. *J. Geophys. Res.* 113, D15112, doi:10.1029/2007JD009618.
- Carslaw, K.S., Harrison, R.G., Kirby, J., 2002. Cosmic rays, clouds, and climate. *Science* 298, 1732-1737, doi: 10.1126/science.1076964.
- Chate, D.M., Murugavel, P., Ali, K., Tiwari, S., Beig, G., 2011. Below-cloud rain scavenging of atmospheric aerosols for aerosol deposition models. *Atmos. Res.* 99, 528-536, doi:10.1016/j.atmosres.2010.12.010.
- Dickinson, R.E., 1975. Solar variability and the lower atmosphere. *Bull. Amer. Meteor. Soc.* 56, 1240-1248, doi:10.1175/1520-0477(1975)056<1240:SVATLA>2.0.CO;2.
- Duell, B., Duell, G., 1948. The behavior of barometric pressure during and after solar particle invasions and solar ultraviolet invasions. *Smithsonian Miscellaneous Collections* 110, 8. Washington: Smithsonian Institution.
- Ermolli, I., Matthes, K., Dudok de Wit, T., Krivova, N.A., Tourpali, K., Weber, M., Unruh, Y.C., Gray, L., Langematz, U., Pilewskie, P., Rozanov, E., Schmutz, W., Shapiro, A., Solanki, S.K., Woods, T.N., 2013. Recent variability of the solar spectral irradiance and its impact on climate modeling. *Atmos. Chem. Phys.* 13, 3945-3977,

doi:10.5194/acp-13-3945-2013.

- Fischer, H.J., Mühleisen, R., 1980. The ionospheric potential and the solar magnetic sector boundary crossings. Rep. Astron. Inst. D-7908, University of Tübingen, Ravensburg, Germany.
- Fleagle, R.G., Businger, J.A., 1980. An Introduction to Atmospheric Physics, 2nd Ed., Academic Press, San Diego.
- Foster, J.C., Vo, H.B., 2002. Average characteristics and activity dependence of the subauroral polarization stream. *J. Geophys. Res.* 107, 1475, doi:10.1029/2002JA009409.
- Gao, X., Li, W., Bortnik, J., Thorne, R.M., Lu, Q., Ma, Q., Tao, X., Wang, S., 2015. The effect of different solar wind parameters upon significant relativistic electron flux dropouts in the magnetosphere, *J. Geophys. Res. Space Phys.* 120, 4324–4337, doi:10.1002/2015JA021182.
- Gray, L.J., Beer, J., Geller, M., Haigh, J.D., Lockwood, M., Matthes, K., Cubasch, U., Fleitmann, D., Harrison, G., Hood, L., Luterbacher, J., Meehl, G.A., Shindell, D., van Geel, B., White, W., 2010. Solar influence on climate. *Rev. Geophys.* 48, RG4001, doi:10.1029/2009RG000282.
- Gringel, W., Rosen, J.M., Hoffman, D.J., 1986. Electrical structure from 0 to 30 kilometers, in: *The Earth's Electrical Environment*. National Academy of Sciences Press, Washington, DC, pp. 166-182.
- Harrison, R.G., Ambaum, M.H.P., 2013. Electrical signature in polar night cloud base variations. *Environ. Res. Lett.* 8, 015027, doi:10.1088/1748-9326/8/1/015027.
- Hebert, L., Tinsley, B.A., Zhou, L., 2012. Global electric circuit modulation of winter cyclone vorticity in the northern high latitudes. *J. Adv. Space Res.* 50, 806-818, <http://dx.doi.org/10.1016/j.asr.2012.03.002>.
- Hines, C.O., Halevy, I., 1977. On the reality and nature of a certain sun-weather correlation. *J. Atmos. Sci.* 34, 382-404.
- Hoppel, W.A., Anderson, R.V., Willett, J.C., 1986. Atmospheric electricity in the planetary boundary layer, in: *The Earth's Electrical Environment*. National Academy of Sciences Press, Washington, DC, pp. 149-165.
- Hurrell, J.W., Kushnir, Y., Ottersen, G., Visbeck, M., 2003. An overview of the North Atlantic oscillation, in: *The North Atlantic Oscillation, Climate Significance and Environmental Impact*. Geophysical Monograph 134, American Geophysical Union, Washington, DC.
- Ineson, S., Scaife, A.A., Knight, J.R., Manners, J.C., Dunstone, N.J., Gray, L.J., Haigh, J.D., 2011. Solar forcing of winter climate variability in the Northern Hemisphere. *Nature Geosci.* 4, 753-757, doi: 10.1038/NNGEO1282.
- IPCC, 2013. *Climate Change 2013: The Physical Science Basis*. Contribution of Working Group I to the Fifth Assessment Report of the Intergovernmental Panel on Climate Change, Stocker, T.F., Qin, D., Plattner, G-K, Tignor, M., Allen, S.K., Boschung, J., Nauels, A., Xia, Y., Bex, V., Midgley, P.M. (Eds.). Cambridge University Press, Cambridge, United Kingdom and New York, NY, USA, doi:10.1017/CBO9781107415324.
- Isaksen, L., Haseler, J., Buizza, R., Leutbecher, M., 2010. The new ensemble of data assimilations. *ECMWF Newslett.* 123, 17-21.
- Kalnay, E., Kanamitsu, M., Kistler, R., Collins, W., Deaven, D., Gandin, L., Iredell, M., Saha, S., White, G., Woollen, J., Zhu, Y., Chelliah, M., Ebisuzaki, W., Higgins, W., Janowiak, J., Mo, K.C., Ropelewski, C., Wang, J., Leetmaa, A., Reynolds, R., Jenne, R., Joseph, D., 1996. The NCEP/NCAR 40-year reanalysis project. *Bull. Amer. Meteor. Soc.* 77, 437-471.
- Kirkby, J., Curtius, J., Almeida, J., 60 others, 2011. Role of sulphuric acid, ammonia and galactic cosmic rays in atmospheric aerosol nucleation. *Nature* 476, 429-435, doi:10.1038/nature10343.
- Kirkland, M.W., Tinsley, B.A., Hoeksema, J.T., 1996. Are stratospheric aerosols the missing link between tropospheric vorticity and Earth transits of the heliospheric current sheet? *J. Geophys. Res.* 101, D23, 29689-29699.
- Kniveton, D.R., Tinsley, B.A., 2004. Daily changes in global cloud cover and Earth transits of the heliospheric current sheet. *J. Geophys. Res.* 109, D11201, doi:10.1029/2003JD004232.
- Lam, M.M., Chisham, G., Freeman, M.P., 2013. The interplanetary magnetic field influences mid-latitude surface atmospheric pressure. *Environ. Res. Lett.* 8, 045001, doi:10.1088/1748-9326/8/4/045001.
- Lam, M.M., Chisham, G., Freeman, M.P., 2014. Solar-wind-driven geopotential height anomalies originate in the Antarctic lower troposphere. *Geophys. Res. Lett.* 41, doi:10.1002/2014GL061421.
- Larsen, M.F., Kelly, M.C., 1977. A study of an observed and forecasted meteorological index and its relation to the interplanetary magnetic field. *Geophys. Res. Lett.* 4(8), 337-340.
- Lean, J., Rind, D., 1998. Climate forcing by changing solar radiation. *J. Clim.* 11, 3069-3094, doi:10.1175/1520-0442(1998)011<3069:CFBCSR>2.0.CO;2.
- Lorentz, E.N., 1963. Deterministic nonperiodic flow. *J. Atmos. Sci.* 20, 130-141.
- Macdonald, N.J., Roberts, W.O., 1960. Further evidence of a solar corpuscular influence on large-scale circulation at 300 mb. *J. Geophys. Res.* 65(2), 529-534.
- Mansurov, S.M., Mansurova, L.G., Mansurov, G.S., Mikhnevich, V.V., Visotsky, A.M., 1974. North-south asymmetry of geomagnetic and tropospheric events. *J. Atmos. Terr. Phys.* 36(1), 1957-1962.
- Markson, R., 1983. Solar modulation of fair-weather and thunderstorm electrification and a proposed program to test an atmospheric electrical Sun-weather mechanism, in: McCormac, B.M. (Ed.), *Weather and Climate Responses to*

- Solar Variations, Colorado Associated University Press, Colorado, pp. 323-343.
- Mironova, I.A., Usoskin, I.G., Kovaltsov, G.A., Petelina, S.V., 2012a. Possible effect of extreme solar energetic particle event of 20 January 2005 on polar stratospheric aerosols: direct observational evidence. *Atmos. Chem. Phys.* **12**, 769-778, doi:10.5194/acp-12-769-2012.
- Mironova, I., Tinsley, B., Zhou, L., 2012b. The links between atmospheric vorticity, radiation belt electrons, and the solar wind. *J. Adv. Space Res.* **50**, 783–790, doi:10.1016/j.asr.2011.03.043.
- Mironova, I.A., Aplin, K.L., Arnold, F., Bazilevskaya, G.A., Harrison, R.G., Krivolutsky, A.A., Nicoll, K.A., Rozanov, E.V., Turunen, E., Usoskin, I.G., 2015. Energetic Particle Influence on the Earth's Atmosphere. *Space Sci. Rev.*, doi:10.1007/s11214-015-0185-4.
- Mühleisen, R., Fischer, H.J., 1987. Das luft-electrische feld in der bodennahen schicht (The atmospheric electric field in the atmospheric layer close to ground) Part 1. Final Report F. V. 335/57, 3125/60, T-265-I-203 and T-499-I-203, Astronomical Institut, Universität Tübingen.
- Newell, R.E., 1983. Comments on the Boulder Solar Terrestrial Symposium, in: McCormac, B.M. (Ed.), *Weather and Climate Responses to Solar Variations*, Colorado Associated University Press, Colorado, pp. 29-30.
- Padgaonkar, A.D., Arora, B.R., 1981. Tropospheric vorticity responses to the solar magnetic sector structure and geomagnetic disturbances. *Pure Appl. Geophys.* **119**, 893-900.
- Page, D.E., 1989. The interplanetary magnetic field and sea level polar atmospheric pressure, in: Avery, S.K., Tinsley, B.A. (Eds.), *Workshop on Mechanisms for Tropospheric Effects of Solar Variability and the Quasi-Biennial Oscillation*, University of Colorado, Boulder, Colorado, USA, p. 227.
- Pettigrew, E.D., Shepherd, S.G., Ruohoniemi, J.M., 2010. Climatological patterns of high-latitude convection in the northern and southern hemispheres: dipole tilt dependencies and interhemispheric comparisons. *J. Geophys. Res.* **115**, A07305, doi:10.1029/2009JA014956.
- Prenni, A.J., Harrington, J.Y., Tjernström M., et al., 2007. Can ice-nucleating aerosols affect arctic seasonal climate? *Bull. Am. Meteorol. Soc.* **88**, 541-550, doi:10.1175/BAMS-88-4-541.
- Pruppacher, H.R., Klett, J.D., 1997. *Microphysics of Clouds and Precipitation*, 2nd Ed., Springer, London, doi:10.1007/978-0-306-48100-0.
- Reichler, T., Kim, J., Manzini, E., Kröger, J., 2012. A stratospheric connection to Atlantic climate variability. *Nature Geosci.* **5**, 783-787. doi:10.1038/ngeo1586.
- Reiter, R., 1977. The electric potential of the ionosphere as controlled by the solar magnetic structure. Result of a study over the period of a solar cycle. *J. Atmos. Terr. Phys.* **39**, 95-99.
- Roberts, W.O., Olsen, R.H., 1973. Geomagnetic storms and wintertime 300-mb trough development in the North Pacific-North America area. *J. Atmos. Sci.* **30**, 135-140.
- Roble, R.G., Tzur, I., 1986. The global atmospheric-electrical circuit, in: *The Earth's Electrical Environment*, National Academy of Sciences Press, Washington, DC, pp. 206-231.
- Roldugin, V.C., Tinsley, B.A., 2004. Atmospheric transparency changes associated with solar-wind-induced atmospheric electricity variations, *J. Atmos. Sol.-Terr. Phys.* **66**(13-14), 1143-1149, doi:10.1016/j.jastp.2004.05.006.
- Rosenfeld, D., Kaufman, Y.J., Koren, I., 2006. Switching cloud cover and dynamical regimes from open to closed Benard cells in response to suppression of precipitation by aerosols. *Atmos. Chem. Phys.* **6**, 2503-2511, doi:10.5194/acp-6-2503-2006.
- Rosenfeld, D., Lohmann, U., Raga, G.B., O'Dowd, C.D., Kulmala, M., Fuzzi, S., Reissell, A., Andreae, M.O., 2008. Flood or drought: how do aerosols affect precipitation? *Science* **321**, 1309-1313, doi: 10.1126/science.1160606.
- Rosinski, J., Morgan, G., 1991. Cloud condensation nuclei as a source of ice-forming nuclei in clouds. *J. Aerosol. Sci.* **22**, 123-133, doi:10.1016/0021-8502(91)90022-A.
- Rossby, C.G., Collaborators, 1939. Relation between variations in the intensity of the zonal circulation of the atmosphere and the displacements of the semi-permanent centers of action. *J. Mar. Res.* **2**, 38-55.
- Rossby C.G., 1940. Planetary flow patterns in the atmosphere. *Quart. J. Roy. Meteor. Soc. (suppl.)* **66**, 68-87.
- Rozanov, E., Calisto, M., Egorova, T., Peter, T., Schmutz, W., 2012. Influence of the precipitating energetic particles on atmospheric chemistry and climate. *Sur. Geophys.* **33**, 483-501, doi 10.1007/s10712-012-9192-0.
- Rycroft, M.J., Nicoll, K.A., Aplin, K.L., Harrison, R.G., 2012. Recent advances in global electric circuit coupling between the space environment and the troposphere, *J. Atmos. Sol.-Terr. Phys.* **90/91**, 198-211, doi:10.1016/j.jastp.2012.03.015.
- Seppälä, A., Matthes K., Randall, C.E., Mironova, I.A., 2014. What is the solar influence on climate? Overview of activities during CAWSES-II. *Prog. Earth Planet. Sci.* **1**:24, doi:10.1186/s40645-014-0024-3.
- Tinsley, B.A., 2008. The global atmospheric electric circuit and its effects on cloud microphysics. *Rep. Prog. Phys.* **71**, 066801, doi:10.1088/0034-4885/71/6/066801.
- Tinsley, B.A., 2010. Electric charge modulation of aerosol scavenging in clouds: rate coefficients with Monte Carlo simulation of diffusion. *J. Geophys. Res.* **115**, D23211, doi:10.1029/2010JD014580.

- Tinsley, B.A., 2012. A working hypothesis for connections between electrically-induced changes in cloud microphysics and storm vorticity, with possible effects on circulation. *J. Adv. Space Res.* 50, 791-805, doi:10.1016/j.asr.2012.04.008.
- Tinsley, B.A., Deen, G.W., 1991. Apparent tropospheric response to MeV-GeV particle flux variations: a connection via electrofreezing of supercooled water in high-level clouds? *J. Geophys. Res.* 96, 22283-22296.
- Tinsley, B.A., Heelis, R.A., 1993. Correlations of atmospheric dynamics with solar activity: evidence for a connection via the solar wind, atmospheric electricity, and cloud microphysics. *J. Geophys. Res.* 98, 10375-10384.
- Tinsley, B.A., Leddon, D.B., 2013. Charge modulation of scavenging in clouds: extension of Monte Carlo simulations and initial parameterization. *J. Geophys. Res. Atmos.* 118, 8612-8624, doi:10.1002/jgrd.50618.
- Tinsley, B.A., Zhou, L., 2006. Initial results of a global circuit model with variable stratospheric and tropospheric aerosols. *J. Geophys. Res.* 111, D16205, doi:10.1029/2005JD006988.
- Tinsley, B.A., Zhou, L., 2015. Parameterization of aerosol scavenging due to atmospheric ionization. *J. Geophys. Res. Atmos.* 120, 8389-8410, doi:10.1002/2014JD023016.
- Tinsley, B.A., Brown, G.M., Scherrer, P.H., 1989. Solar variability influences on weather and climate: possible connections through cosmic ray fluxes and storm intensification. *J. Geophys. Res.* 94, 14783-14792.
- Tinsley, B.A., Hoeksema, J.T., Baker, D.N., 1994. Stratospheric volcanic aerosols and changes in air-earth current density at solar wind magnetic sector boundaries as conditions for the Wilcox tropospheric vorticity effect. *J. Geophys. Res.* 99, D8, 16805-16813, doi:10.1029/94JD01207.
- Tinsley, B.A., Rohrbaugh, R.P., Hei, M., Beard, K.V., 2000. Effects of image charges on the scavenging of aerosol particles by cloud droplets and on droplet charging and possible ice nucleation processes. *J. Atmos. Sci.* 57, 2118-2134.
- Tinsley, B.A., Rohrbaugh, R.P., Hei, M., 2001. Electroscavenging in clouds with broad droplet size distributions and weak electrification. *Atmos. Res.* 59-60, 115-135.
- Tinsley, B.A., Zhou, L., Plemmons, A., 2006. Changes in scavenging of particles by droplets due to weak electrification in clouds. *Atmos. Res.* 79, 266-295, doi:10.1016/j.atmosres.2005.06.004.
- Tinsley, B.A., Zhou, L., Liu, W., 2012. The role of volcanic aerosols and relativistic electrons in modulating winter storm vorticity. *J. Adv. Space Res.* 50, 819-827, doi:10.1016/j.asr.2011.12.019.
- Todd, M.C., Kniveton, D.R., 2001. Changes in cloud cover associated with Forbush decreases of galactic cosmic rays. *J. Geophys. Res.* 106 (D23), 32031-32041, doi:10.1029/2001JD000405.
- Torreson, O.W., Parkinson, W.C., Gish, O.H., Wait, G.R., 1946. Ocean atmospheric-electric results (Scientific Results of Cruise VII of the Carnegie During 1928-1929 Under Command of Captain J. P. Ault, vol. 3). Carnegie Institute of Washington Publication, vol. 568, p136.
- Tripathi, S.N., Harrison, R.G., 2002. Enhancement of contact nucleation by scavenging of charged aerosol particles. *Atmos. Res.* 62, 57-70, doi:10.1016/S0169-8095(02)00020-0.
- Tripathi, S.N., Vishnoi, S., Kumar, S., Harrison, R.G., 2006. Computationally efficient expressions for the collision efficiency between electrically charged aerosol particles and cloud droplets. *Q. J. R. Meteorol. Soc.* 132, 1717-1731, doi: 10.1256/qj.05.125.
- Tzur, I., Roble, R.G., Zhuang, H.C., Reid, G.C., 1983. The response of the Earth's global electric circuit to a solar proton event, pp.427-435, in "Weather and Climate Responses to Solar Variations", McCormac, B.M. (Ed.), Colorado Associated University Press.
- Vangengeim, G.Ya, Girs, A.A., 1964. Katalog makrosinopticheskikh protsessov po klassifikatsii G.Ya Vangengeima (Catalog of Macrosynoptic Processes according to the Vangengeim Classification), Leningrad: AANII.
- Veretenenko, S., Thejll, P., 2004. Effects of energetic solar proton events on the cyclone development in the North Atlantic. *J. Atmos. Sol.-Terr. Phys.* 66, 393-405, doi:10.1016/j.jastp.2003.11.005.
- Veretenenko, S., Thejll, P., 2005. Cyclone regeneration in the North Atlantic intensified by energetic solar proton events. *Adv. Space Res.* 35, 470-475, doi:10.1016/j.asr.2005.01.079.
- Veretenenko, S., Thejll, P., 2013. Influence of energetic Solar Proton Events on the development of cyclonic processes at extratropical latitudes. *J. Physics: Conf. Ser.* 409, doi:10.1088/1742-6596/409/1/012237.
- Vonnegut, B., Moore, C.B., Semonin, R.G., Bullock, J.W., Staggs, D.W., Bradley, W.E., 1962. Effect of atmospheric space charge on initial electrification of cumulus clouds, *J. Geophys. Res.* 67(10), 3909-3922.
- Weimer, D.R., 1996. A flexible, IMF dependent model of high latitude electric potentials having "space weather" applications. *Geophys. Res. Lett.* 23(18), 2549-2552.
- Wilcox, J.M., Scherrer, P.H., Svalgaard, L., Roberts, W.O., Olsen, R.H., 1973. Solar magnetic sector structure: relation to circulation of the Earth's atmosphere. *Science* 180, 185-186.
- Wilks, D.S., 2006. On 'field significance' and the false discovery rate. *J. Appl. Meteorol. Clim.* 45, 1181-1189.
- Williams, E.R., 2005. Lightning and climate: a review. *Atmos. Res.* 76, 272-287, doi:10.1016/j.atmosres.2004.11.014.
- Willis, D.M., 1976. The energetics of Sun-weather relationships: magnetospheric processes. *J. Atmos. Terr. Phys.* 38, 685-698.

- Zhou, L., Tinsley, B.A., 2007. Production of space charge at the boundaries of layer clouds. *J. Geophys. Res.* 112, D11203, doi:10.1029/2006JD007998.
- Zhou, L., Tinsley, B.A., 2012. Time dependent charging of layer clouds in the global electric circuit. *Adv. Space Res.* 50, 828-842, doi:10.1016/j.asr.2011.12.018.
- Zhou, L., Tinsley, B.A., Huang, J., 2014. Effects on winter circulation of short and long term solar wind changes. *J. Adv. Space Res.* 54, 2478-2490, doi:10.1016/j.asr.2013.09.017.
- Zhou, L., Tinsley, B.A., Plemmons, A., 2009. Scavenging in weakly electrified saturated and subsaturated clouds, treating aerosol particles and droplets as conducting spheres. *J. Geophys. Res.* 114, D18201, doi:10.1029/2008JD011527.

Figure 1. Schematic of a section through the global atmospheric electric circuit (GEC). The circuit is mostly driven by the internal meteorological generator associated with thunderstorms and electrified clouds. Each of about 1000 highly-electrified storms around the globe sends about 1 ampere to the ionosphere, charging it to a voltage $V_i \sim 250$ kV. If R_M , and R_T are the column resistances ($\Omega\text{-m}^2$) of the middle atmosphere and troposphere respectively, then the local downward current density, J_z , is given by Ohm's Law in three dimensions: $J_z = V_i / (R_M + R_T)$. Any change in V_i , R_M , or R_T affects J_z . R_M and R_T vary with cosmic ray flux, relativistic electron flux, and solar proton flux. V_i varies diurnally (the Carnegie variation) and with IMF and solar wind speed changes. Volcanic aerosols, as well as energetic particles, affect R_M and R_T , with all acting together to modulate the ionosphere-earth current density J_z . Adapted from Mühleisen and Fischer (1967).

Figure 2. Connections of weather and climate with thunderstorms, solar activity, and galactic cosmic ray flux, via the global atmospheric electric circuit and cloud and aerosol microphysics. Six independent forcing agents (A through F) are shown that affect the ionosphere-earth current density J_z . Day-to-day meteorological responses correlate independently with each of these inputs. The responses are: A - the Mansurov effect; B - the Burns effect; C and F - the Roberts, Pudovkin, and Egorova effects; D - the Wilcox, Kniveton, Roldugin, and Misumi effects; and E - the Schuurmans and Veretenenko effects. The Mansurov, Burns, Roberts, Wilcox and Veretenenko effects are discussed in section 2. The hypothesized cloud microphysical and macroscopic processes that connect J_z and the meteorological responses are indicated in the fifth and sixth row of boxes, and are discussed in section 3. Adapted from Tinsley (2008).

Figure 3. The Mansurov Effect. This is a high-latitude anomaly in the surface atmospheric pressure, driven by variability in the solar-wind-driven ionospheric electric potential, V : (a) The zonal mean anomaly in the 12 UT surface pressure from 1999-2002 NCEP/NCAR reanalysis data for two distinctly different states of the interplanetary magnetic field (IMF), namely, when the daily average of IMF $B_y \geq 3$ nT (red) and when the daily average of IMF $B_y \leq -3$ nT (blue). The four-year zonal mean of the pressure anomaly has been removed before plotting. Both these IMF states contain $\sim 20\%$ of IMF measurements; (b) the difference between the red and blue lines in panel (a). Error bars indicate the error in the mean in (a) and (b); (c) The probability output from a Wilcoxon Rank-Sum (WRS) test between the two IMF B_y states shows that the zonal-mean Mansurov effect is most significant poleward of 50° – 60° latitude; The difference between the solar-wind-driven ionospheric electric potential for IMF B_y large and positive and IMF B_y large and negative in (d) the northern hemisphere, and (e) the southern hemisphere according to the model of Pettigrew et al. (2010), is approximately circularly symmetric about the geomagnetic pole and displaced from the geographic pole. Adapted from Lam et al. (2013).

Figure 4. The dependence of the high-latitude ionospheric potential difference (PD) on interplanetary magnetic field (IMF). The figure shows the dependence of the *daily-averaged* solar-wind-induced ionospheric potential differences at Vostok on *daily-averaged* interplanetary magnetic field. The dependences are shown for (a) B_y and (b) B_z . The data cover the interval from 2000 to 2001. The overhead potential changes were derived from simultaneous satellite IMF measurements, using the Weimer (1996) model. Reproduced from Burns et al. (2007).

Figure 5. Schematic of the superposition of the solar-wind-driven ionospheric potential difference on the thunderstorm-driven ionosphere-to-ground potential difference. Top: shown for IMF $B_z = -5.5$ nT, $B_y = 0$, (adapted from Markson, 1983), and also shown as dashed line in bottom plot. Bottom: the dependence of the ionosphere-to-ground potential difference on IMF B_y for $B_z = -5.5$ nT at high latitudes (adapted from Tinsley and Heelis, 1993).

Figure 6. In Antarctica, the Mansurov effect is greatest in the troposphere and at the base of the stratosphere. (a) The difference in the 1999-2002 mean geopotential height anomaly between IMF $B_y \geq 3$ nT and IMF $B_y \leq -3$ nT states, for the region poleward of 70°S using NCEP/NCAR reanalysis data. A minimum (winter) pressure level for the Antarctic tropopause of 230 hPa is marked by the horizontal grey dashed line; (b) as for (a) but masked at the 1% field significance level (Wilks, 1996) showing that the correlation is most statistically-significant within the troposphere and at the base of the stratosphere. At any given pressure level, the peak correlation occurs at a positive time lag, consistent with the solar-wind-driven ionospheric electric field fluctuations leading the atmospheric response; (c) the results from (b) are plotted at different pressure levels, with a +3 m offset between each decreasing pressure level to aid visualization. Statistically-significant values at the 1% level are plotted in black and values of less statistical significance are plotted in orange. Starting with the line plotted at the bottom of the panel, the levels are 1000, 925, 850, 700, 600, 500, 400, 300 and 250 hPa. The temporally broad peaks shift to increased time lags with increasing altitude, suggestive of an upward propagation of the Mansurov effect from the lower to upper troposphere. Reproduced from Lam et al. (2014).

Figure 7. Dependency of surface pressure on ionospheric electric potential. The dependences of observed surface pressure anomalies on the external (IMF B_y) driver and on the internal thunderstorm driver. The dependences are very similar when derived from mean station values above 83° magnetic latitude. As in Fig. 5, the values of ionospheric potential change for the external driver were derived from the Weimer (1996) model. The ionospheric potential change for the internal driver was obtained from measurements of the vertical electric field at Vostok. Reproduced from Burns et al. (2008).

Figure 8. Correlation of cloud base height with the ‘Carnegie curve’ variation. The mean anomaly in winter cloud base height for Halley (2003-2011) in the Antarctic (blue) and for Sodankylä (2006-2011) in the Arctic (red), plotted against the anomaly in diurnal changes in vertical electric potential gradient PG. The data used at both sites were for very stable meteorological conditions. The Halley data used were for days where the daily mean wind speed was in the lowest decile. Reproduced from Harrison and Ambaum (2013).

Figure 9. Pronounced pressure deviations are associated with Forbush decreases at climatic fronts. Superposed epoch analysis maps of geopotential height variations of the 1000 hPa level in the (a) northern and (b) southern hemispheres on the 4th day after Forbush decrease onsets. Climatic positions of the main atmospheric fronts, which are regions of intensive cyclonic activity, are shown for January. The grey lines indicate the areas of statistical significance according to Monte-Carlo tests: the solid and dashed lines correspond to the significance levels 0.95 and 0.99, respectively. Reproduced from Artamonova and Veretenenko (2014).

Figure 10. Accumulation of electric space charge. Accumulation of electric space charge at layer cloud boundaries, due to the flow of vertical current density (J_z) through vertical gradients in conductivity, and accumulation of space charge in the layer of haze, fog and sea-spray aerosol within a few hundred metres of the ocean surface. This is lifted by updrafts into the body of cyclones, polar lows, and other convective clouds. Adapted from Tinsley (2012).

Figure 11. Numerical modeling of particle scavenging by water droplets. The effect of droplet charge Q (horizontal axis, from $-100e$ to $+100e$), and particle charge q (vertical axis, from $1e$ to $50e$) on collision rate coefficients for three particle radii ($0.01\ \mu\text{m}$, $0.04\ \mu\text{m}$, and $1.5\ \mu\text{m}$) color coded by the value of $F = \log(R_{Q,q}/R_{0,0})$. $R_{Q,q}$ is the rate coefficient for droplet charge Q and particle charge q , and $R_{0,0}$ is the rate coefficient for zero droplet and particle charges. Note the changing color scale representing the F values in each panel, with much larger amplitudes for the smaller particles. Adapted from Tinsley and Zhou (2015).

Figure 12. Future modeling. The needs for quantitative modeling, to test which of the pathways from cloud electrification to macroscopic cloud and dynamical changes are most effective, and to test them quantitatively against observations.

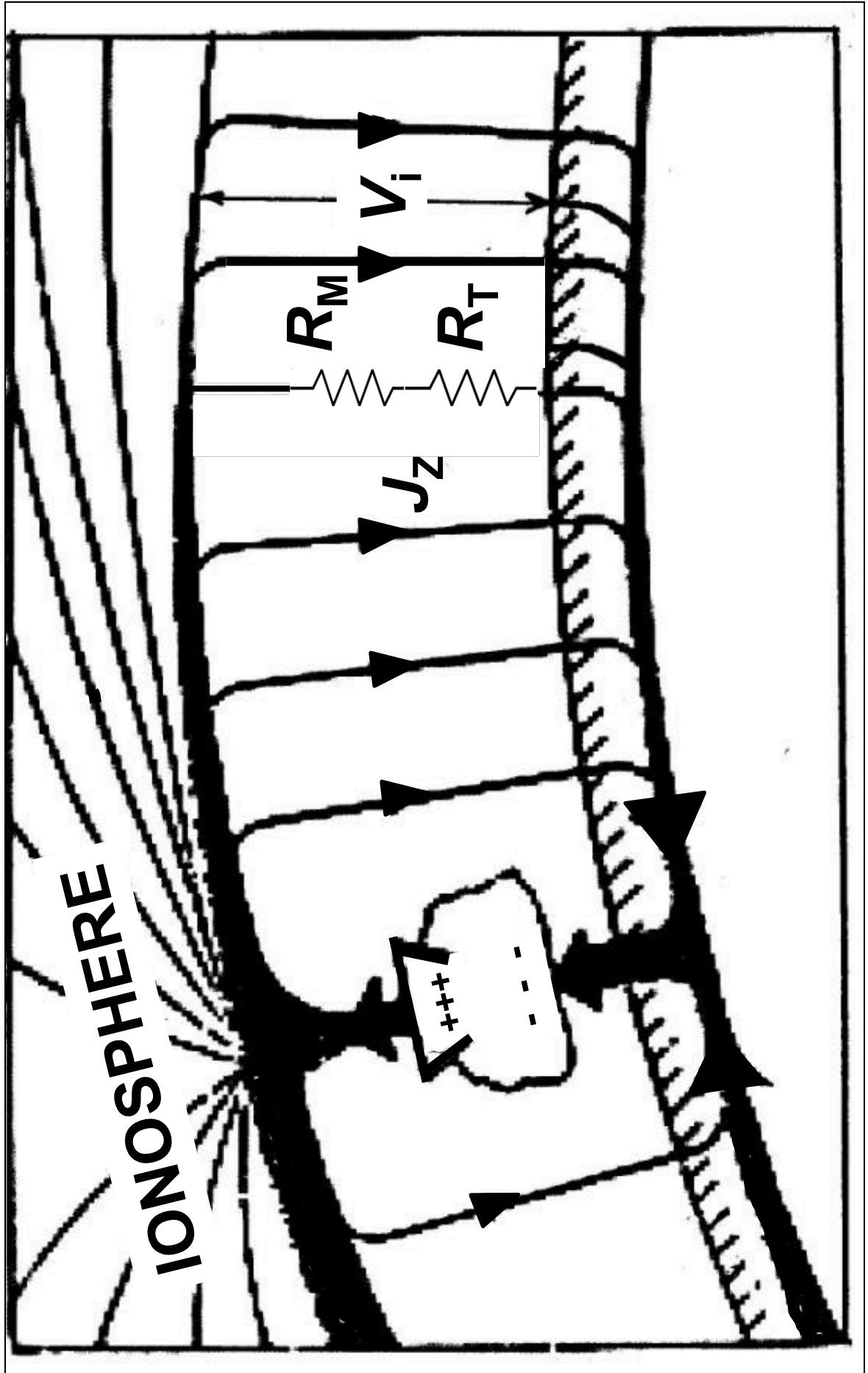
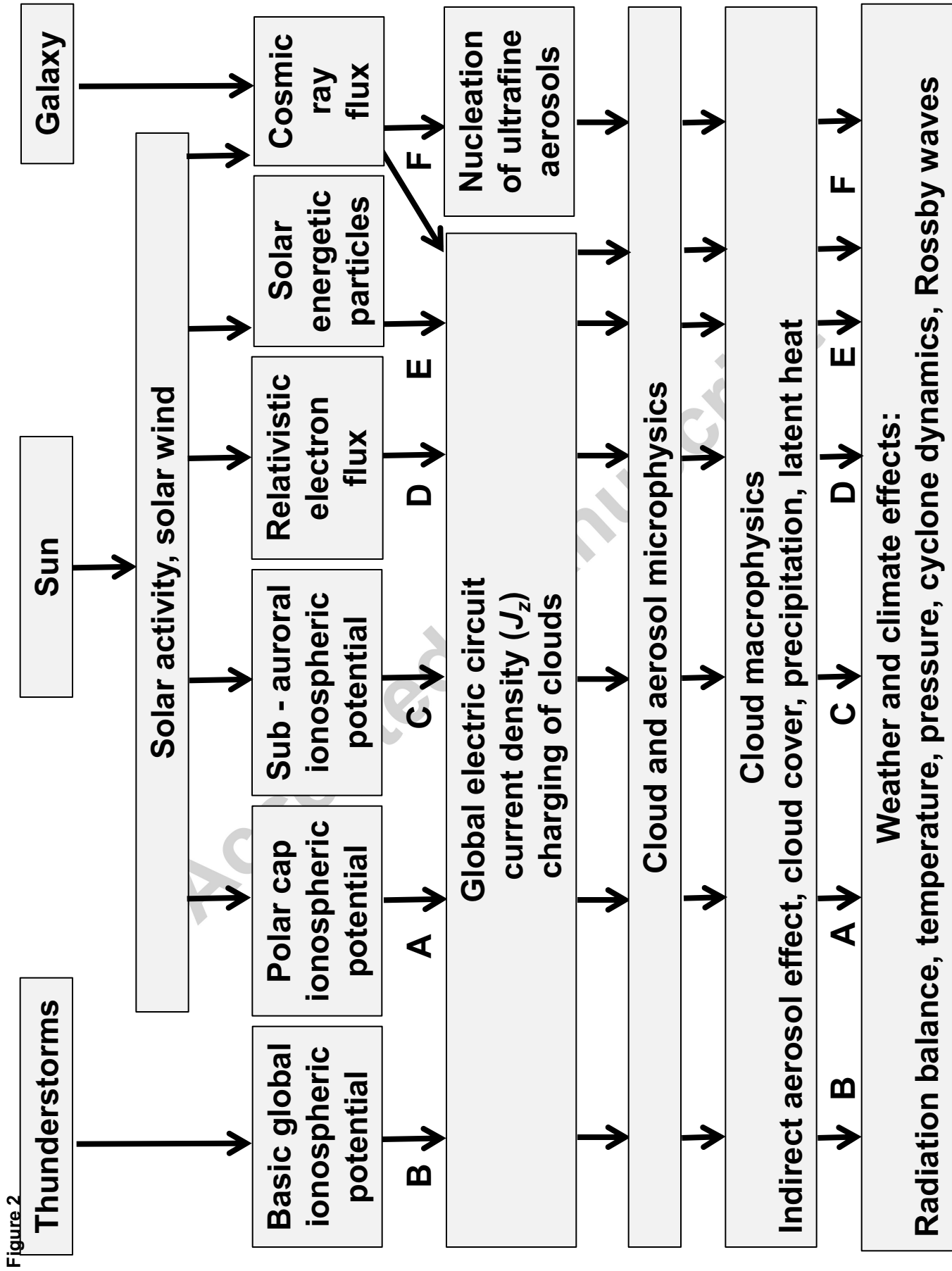
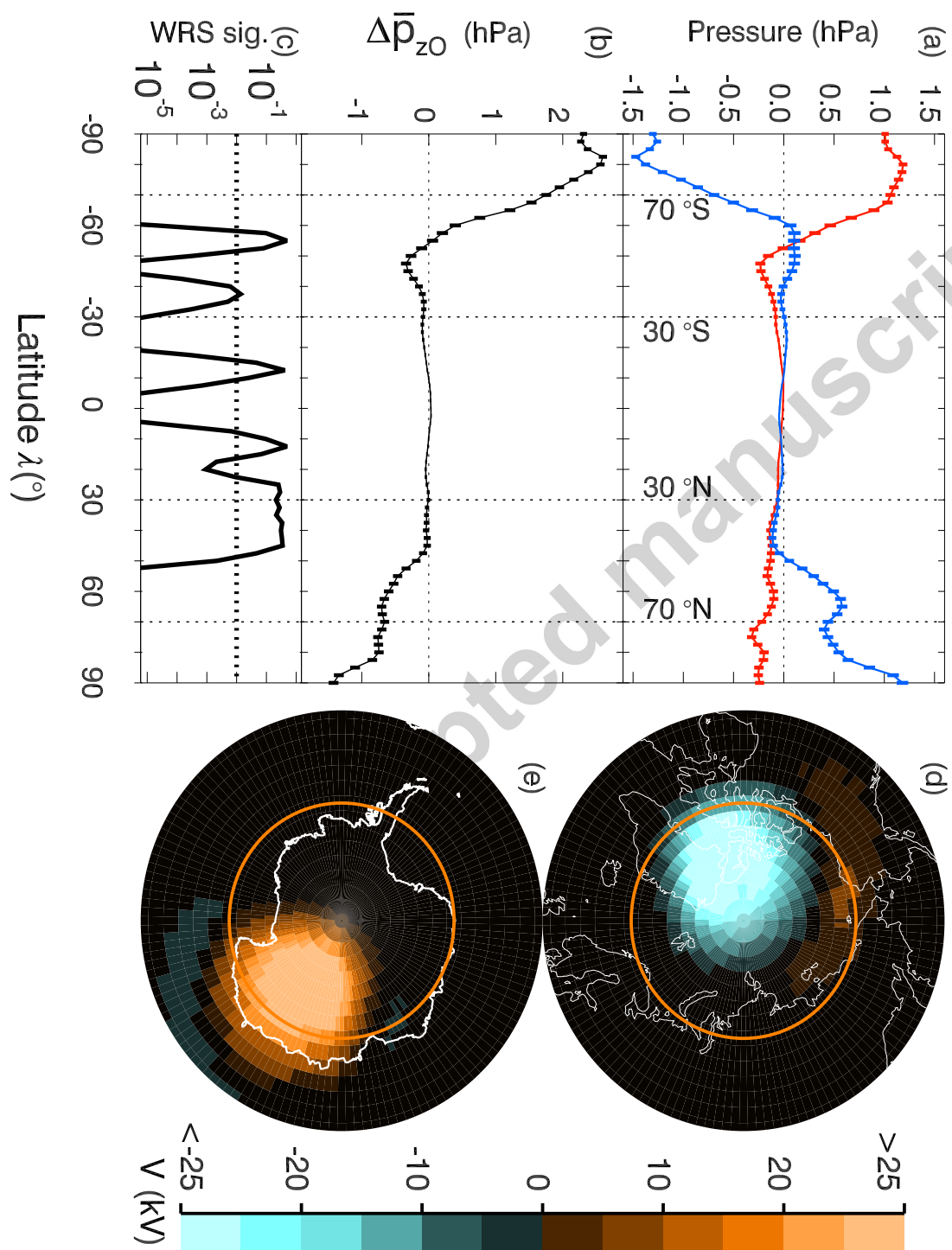
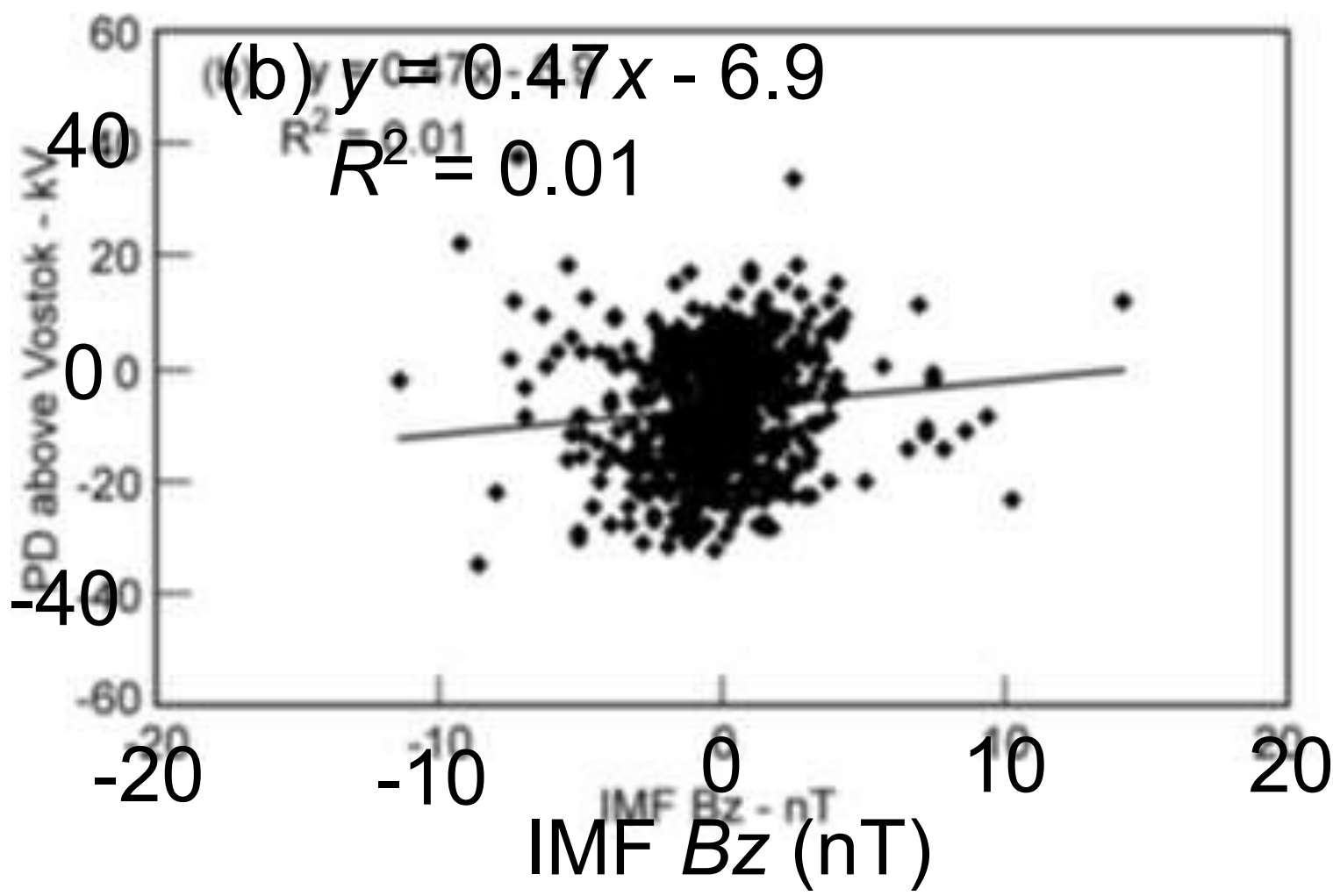
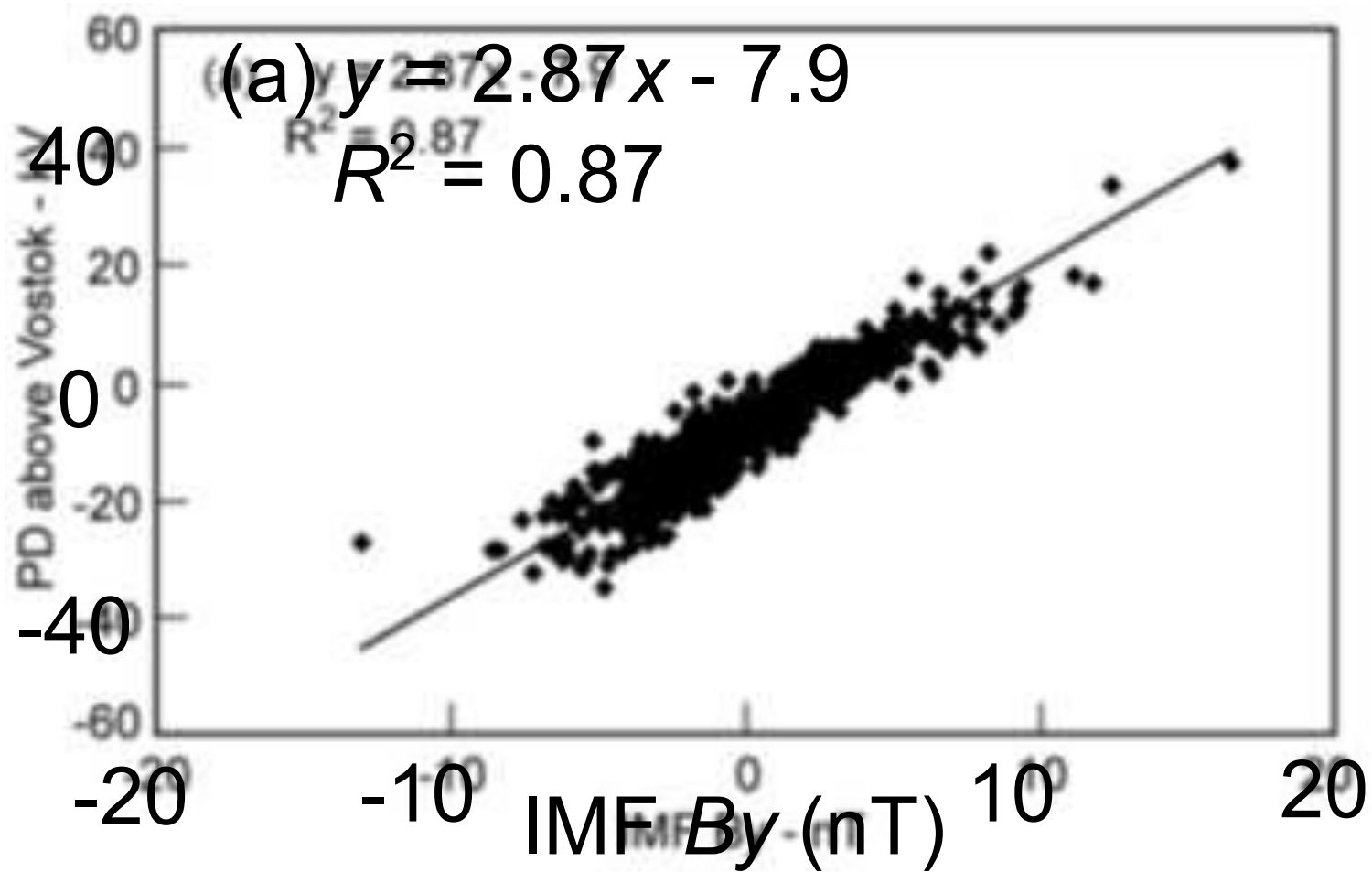


Figure 1





PD above Vostok (kV)



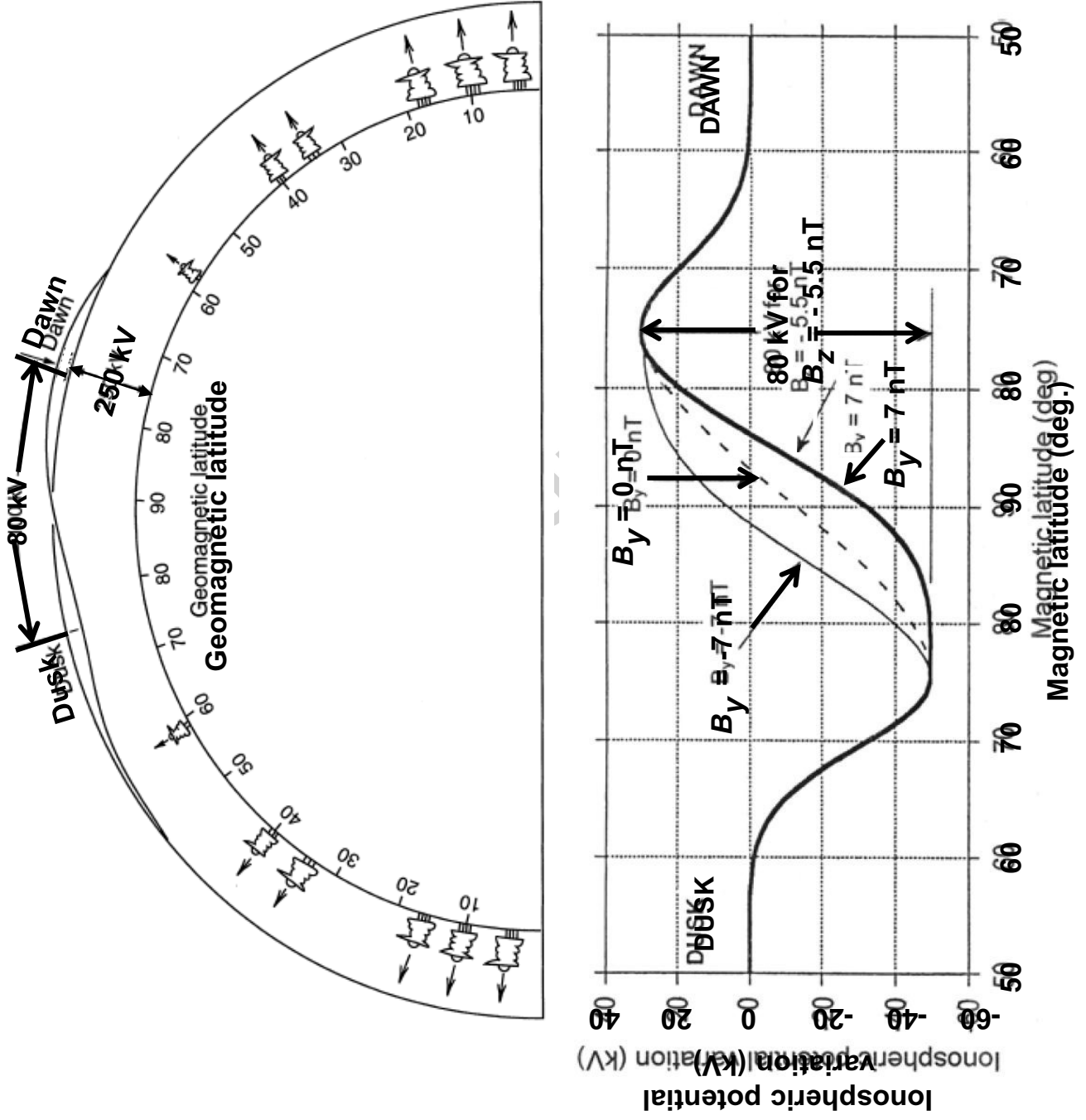
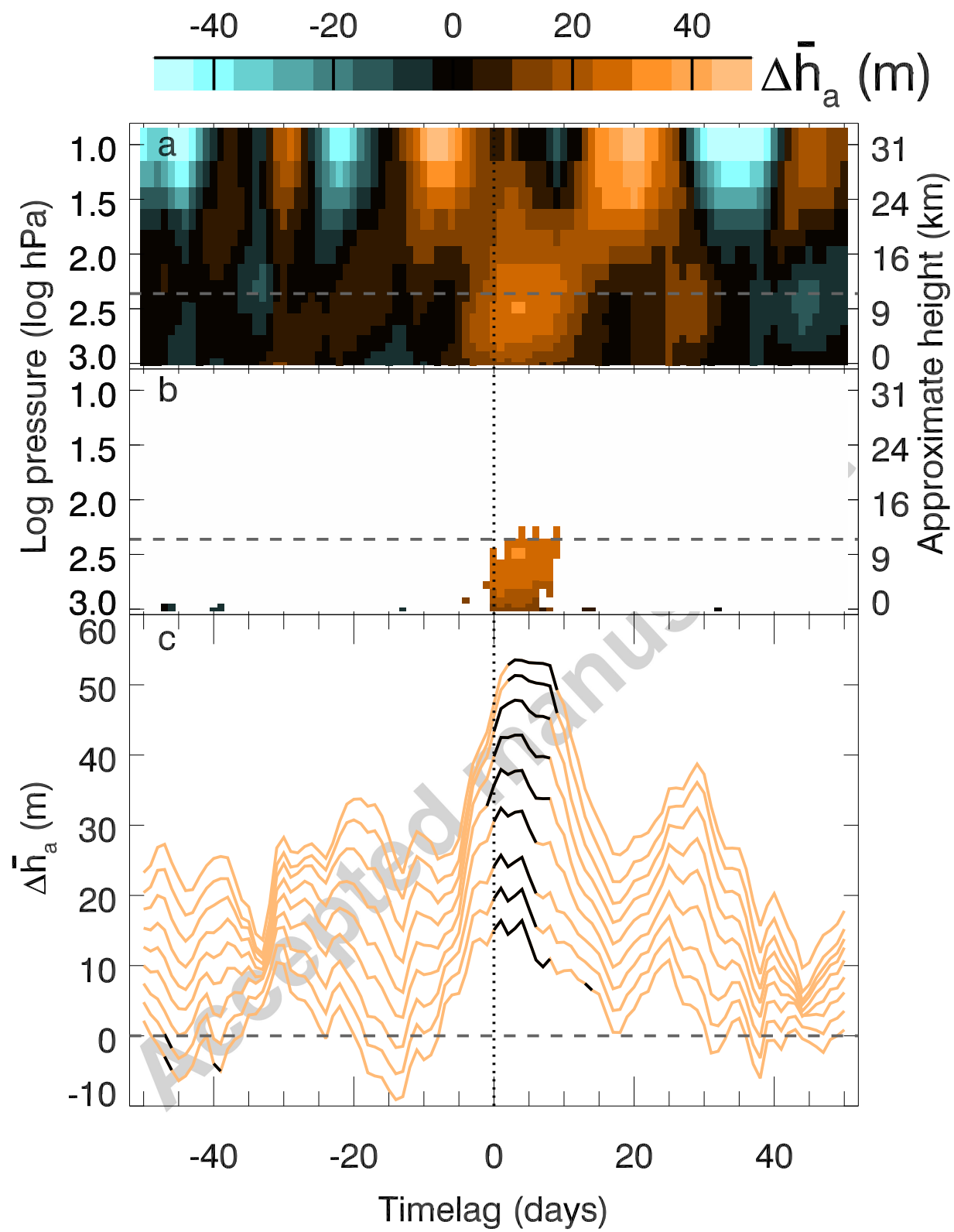
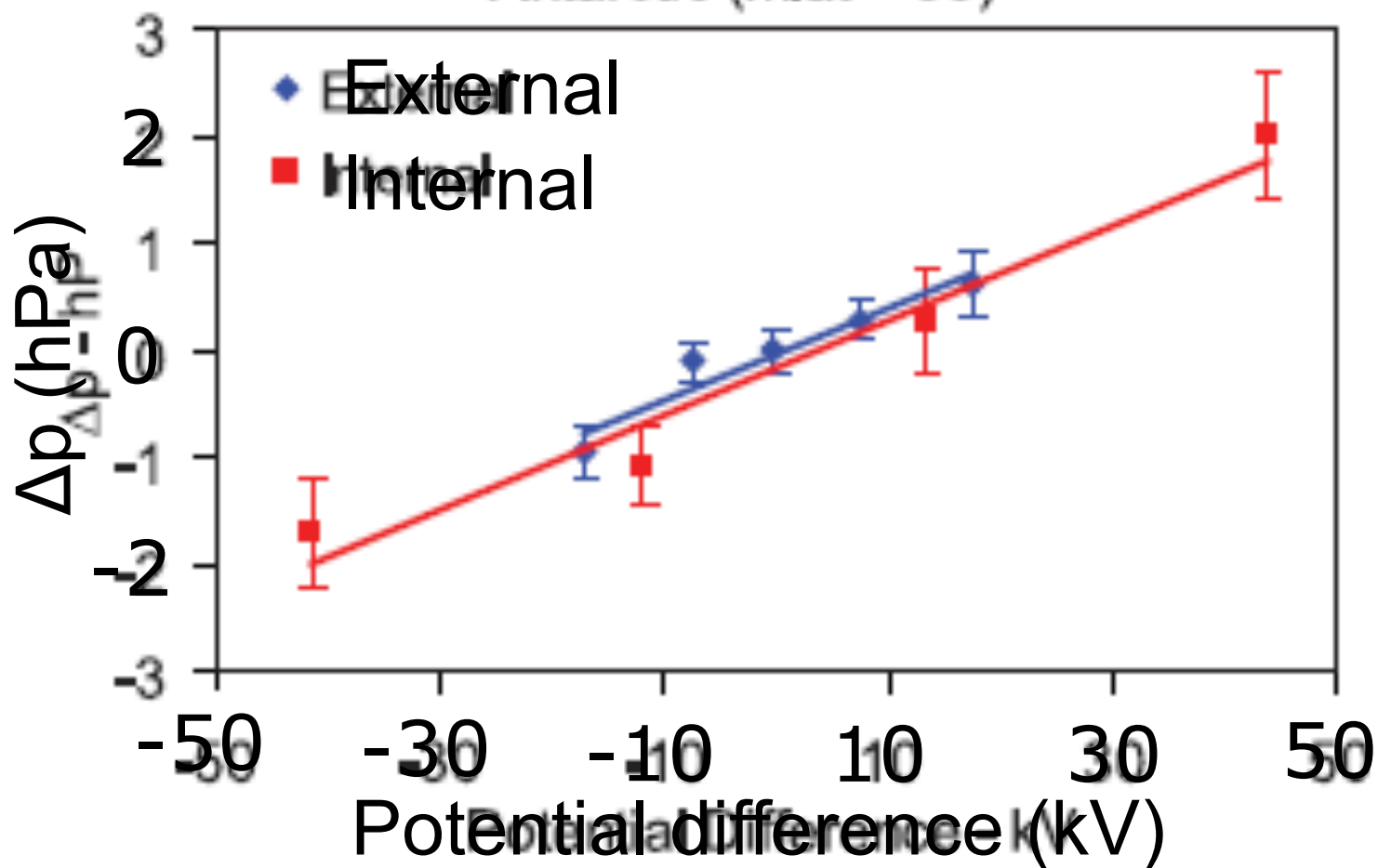
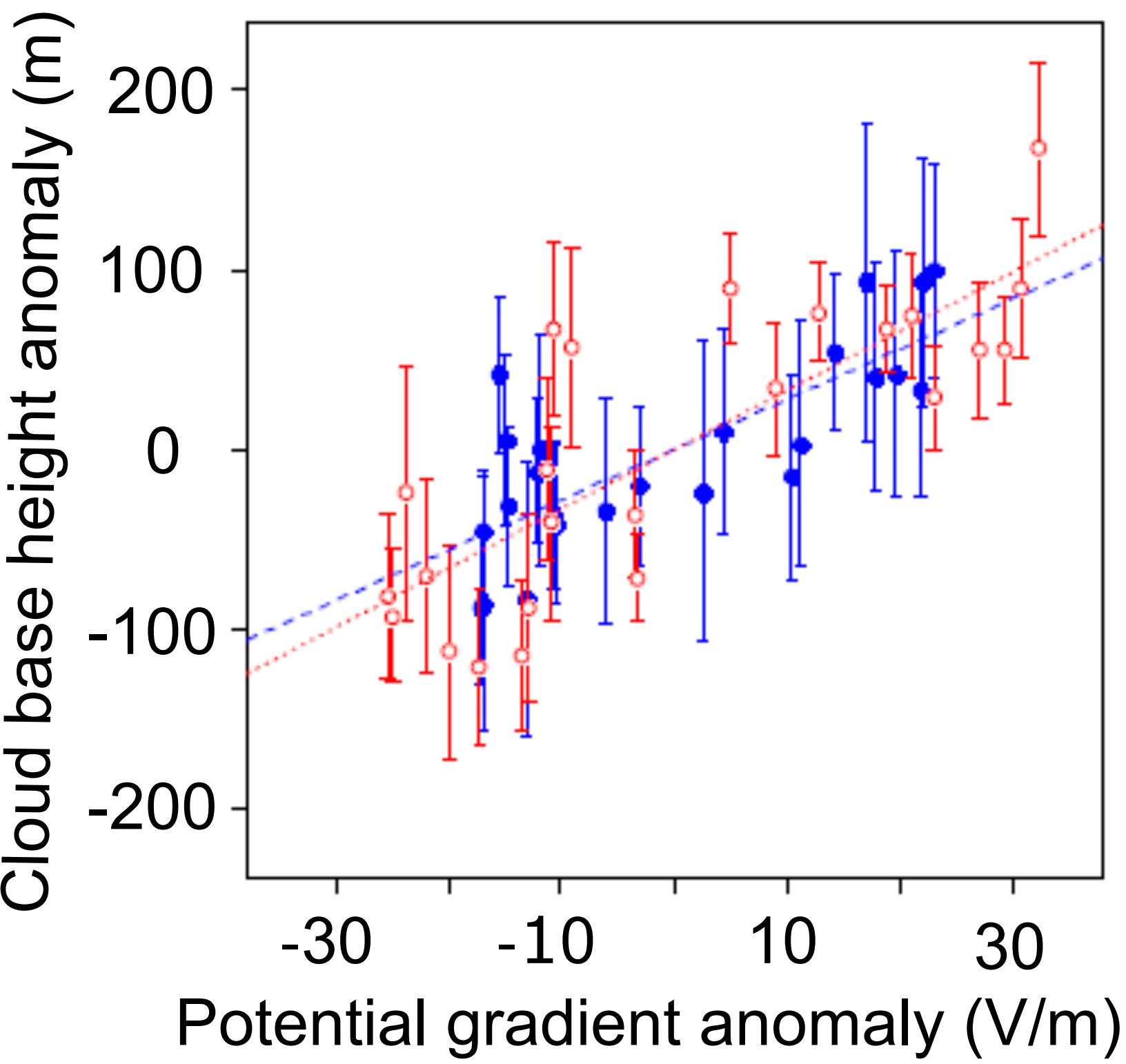


Figure 5



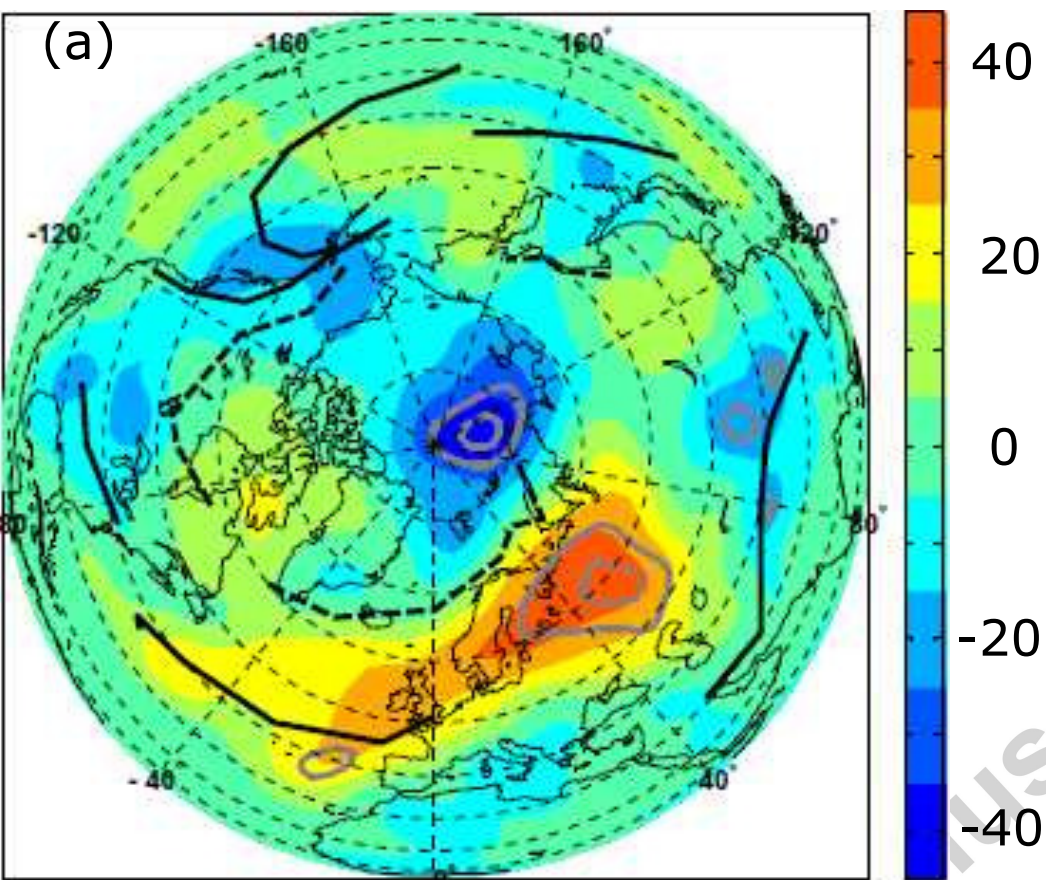
Antarctic (mlat > 83)





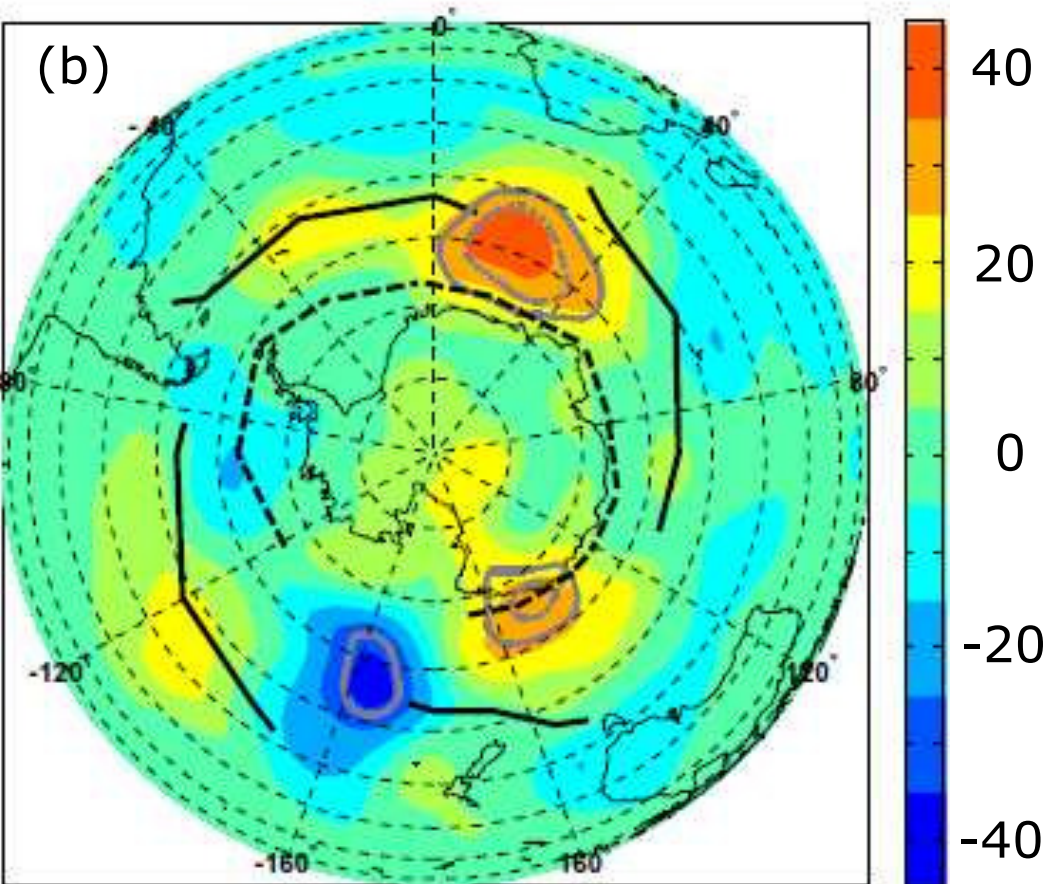
Polar front

Arctic front



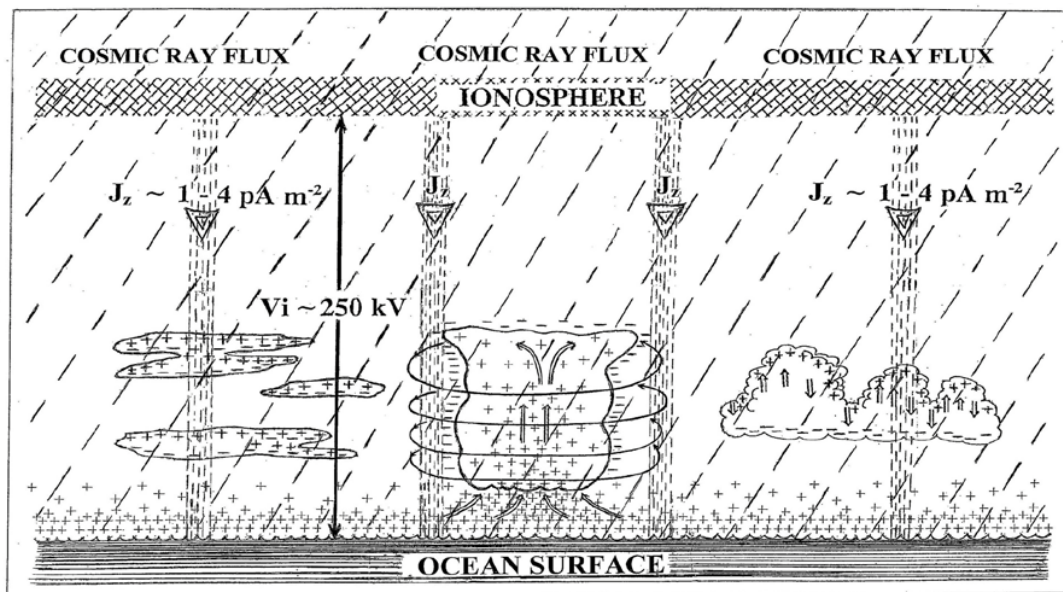
— Polar front - - - - - Arctic front

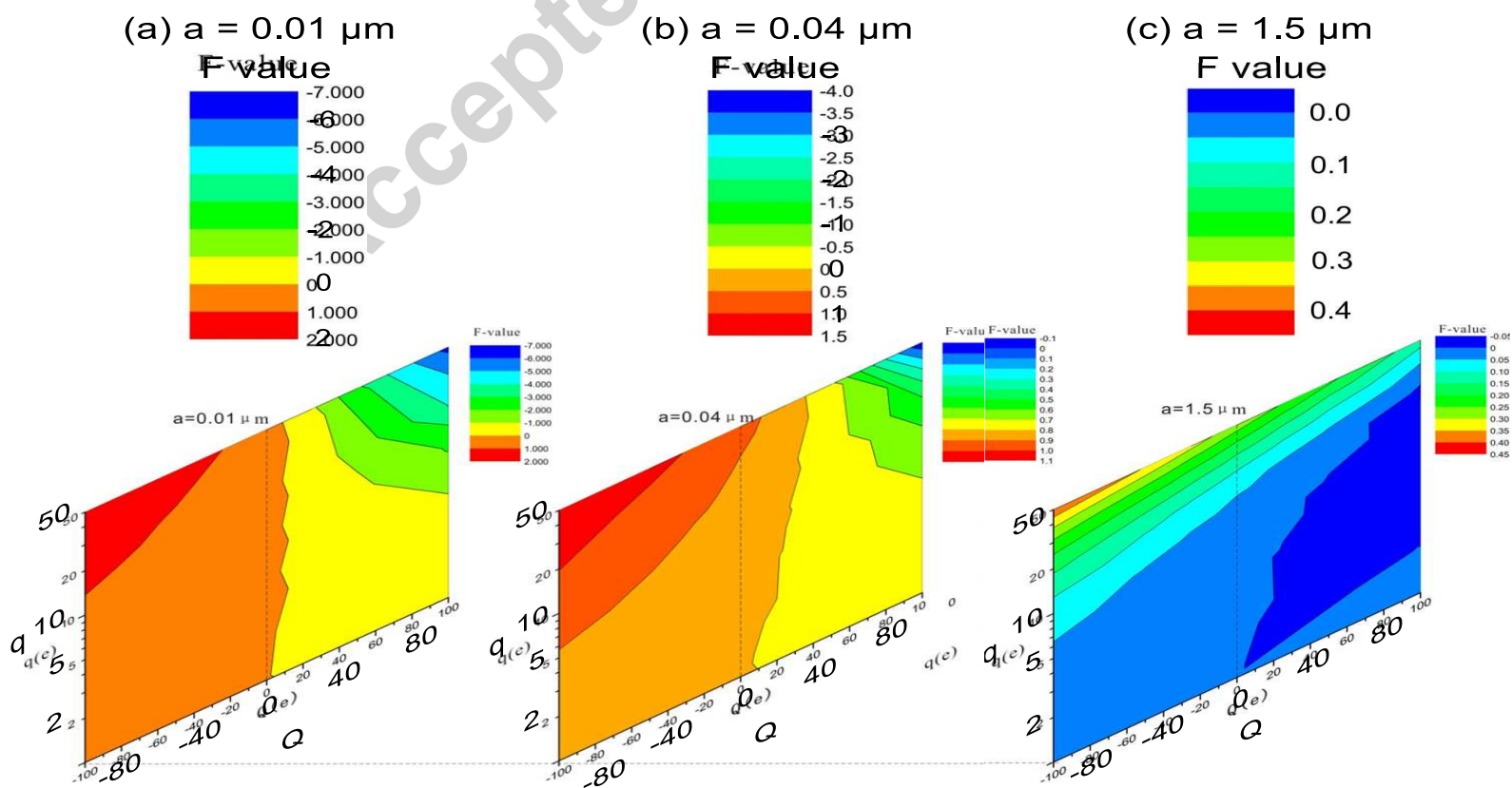
gp.m



— Polar front

- - - - - Antarctic front





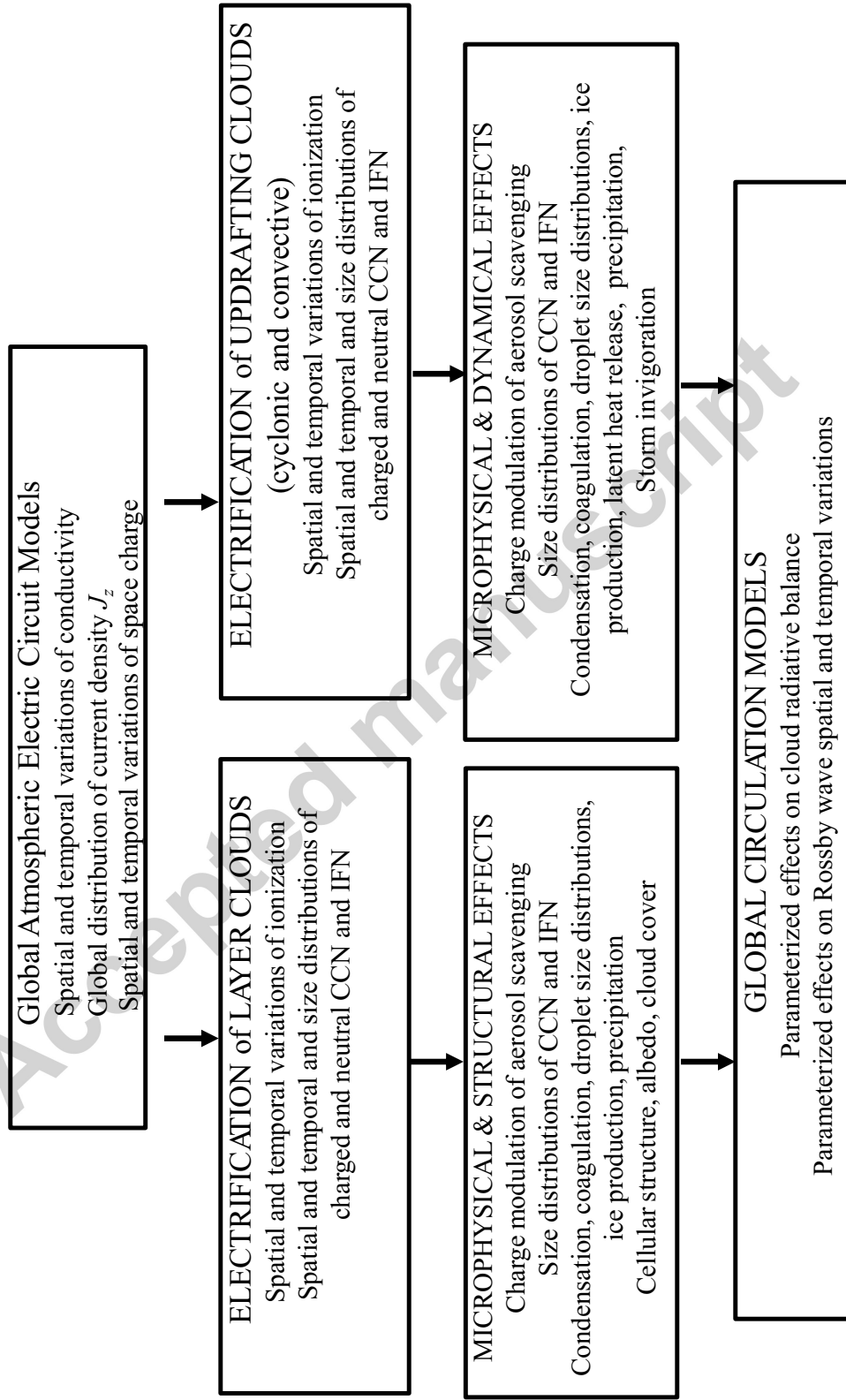


Figure 12